

Politecnico di Torino

Master's Degree Thesis in Automotive Engineering A.Y. 2024/2025 Graduation Session 21 November 2025

Techno-Economic and Environmental Impact Analysis of Electrified Road Systems for Battery Electric Trucks

Supervisors:

Candidate:

Prof. Ezio Spessa

Micaela Boscia - 334093

Prof. Trentalessandro Costantino

Prof. Federico Miretti

"Enjoy the butterflies, enjoy being naive.
Enjoy the nerves, the pressure, people not
knowing your name.
Enjoy the process of making a name
for yourself [...] meeting some great people
along the way.
Bring friends along. Bring family along.
Don't assume they'll be a distraction.
Don't be afraid to surround yourself with people
you care about and love."

- Daniel Ricciardo, 2021

Acknowledgements

I would like to express my sincere gratitude to Professor Spessa for giving me the opportunity to work on this thesis, which represents an important step towards the future of the freight transport sector.

I am also deeply thankful to Professor Miretti and Professor Costantino for their guidance and constant availability throughout the development of this work. Their advice and support were fundamental in bringing this project to completion.

Moving to the personal sphere, my profound appreciation goes to my parents and brother. Thank you for constantly encouraging me to keep going, as long as it made me happy, and for always being by my side.

A special acknowledgement goes to my classmates, who made this academic journey lighter and more enjoyable. The shared struggles and laughter will always be an enduring memory.

Lastly, but by no means least, I would like to thank Federico, my greatest love. We have grown up together, facing both incredible moments and challenges that once seemed insurmountable. Thank you for standing by me and believing in me even when I couldn't believe in myself.

Summary

In recent years, the European Commission has imposed more stringent regulations on CO_2 emissions, requiring significant reductions for Heavy-Duty Vehicles (HDV). For this reason, Battery Electric Trucks (BETs) are becoming a promising solution. While in urban delivery missions the limitations related to payload reduction due to battery weight and restricted driving range are relatively contained, their adoption for long-haul transport remains constrained by long charging times and significant payload penalties. These challenges have driven research into new technologies that allow recharging while driving: the Electrified Road System (ERS).

This thesis evaluates the technical and sustainable feasibility, both environmental and economic, of Dynamic Wireless Power Transfer (DWPT) ERS to address the challenges of long-haul battery electric heavy-duty trucks (BEHDT) along a 715 km route between Torrazza (Piedmont) and Colleferro (Lazio). To this end, MATLAB was used to simulate energy consumption and recharging system utilisation ratios. Subsequently, the environmental impacts were assessed in SimaPro, focusing on the CO_2 emission from the construction of the electrified road over its lifetime. Finally, a Total Cost of Ownership (TCO) analysis was performed through a cost model in Python.

Results show that the implementation of ERS technology enables battery down-sizing up to 46%, reducing the battery's climate impact by approximately 45%. The most significant climate impact arises from road maintenance activities. The TCO analysis, expressed in $\epsilon/ton \cdot km$, indicates that the ERS becomes economically feasible under the average and optimistic scenarios, further demonstrating the advantage of an increased maximum payload enabled by battery downsizing.

In conclusion, the Electrified Road System appears promising for reducing battery size and environmental impact. Nonetheless, cost reductions and high utilisation of the infrastructure are required for large-scale deployment and to ensure economic viability.

Table of Contents

Li	st of	Tables	IX
Li	st of	Figures	Х
A	crony	ms X	III
1	Intr	oduction	1
	1.1	CO ₂ European Legislations for Heavy-Duty Vehicles	1 2
	1.2	Aim and Scope of the Thesis	3
	1.3	Structure of the Thesis	4
2	Fun	lamental Elements of the Thesis	5
	2.1	Battery Electric Truck	5
			6
		2.1.2 Battery Equivalent Circuit Model	7
	2.2		8
		2.2.1 Contact Charging	10
		2.2.2 Dynamic Wireless Power Transfer	11
	2.3	·	13
	2.4		14
		-	15
		2.4.2 Maintenance Cost	15
			15
		2.4.4 Taxes and Fees	15
			16
		OV .	17
3	Cas	Study	19
	3.1		- 19
	3.2		$\frac{1}{20}$

	3.3	Mission Profile
		3.3.1 Road Grade
		3.3.2 Speed Profile
		3.3.3 Stops
	3.4	Battery Charging During Stops
	3.5	Slow Battery Charging
	3.6	Simulation Results
		3.6.1 Correct Functioning of the Simulation
		3.6.2 Battery Downsizing
4	т :С-	Cools Assessment
4		Cycle Assessment 35
	4.1	Goal and Scope
	4.2	Method
		4.2.1 Functional Unit (FU)
	4.0	4.2.2 System Boundary
	4.3	LCI
		4.3.1 Asphalt
		4.3.2 DWPT
	4 4	4.3.3 Energy Delivered
	4.4	Impact Assessment and Interpretation
		4.4.1 Asphalt
		4.4.2 DWPT
		4.4.3 1 km of ERS
		4.4.4 Energy Delivered
		4.4.5 Comparison Between BET and DWPT
5	Tota	al Cost of Ownership 57
	5.1	Scenarios and Data
	5.2	TCO Results
		5.2.1 Total Cost of Ownership
		5.2.2 Purchase Cost Breakdown 61
		5.2.3 Energy Carrier Cost Breakdown
		5.2.4 BET and DWPT TCO Parity Analysis 62
6	Con	aclusions 65
U		
	0.1	Future Works
\mathbf{Bi}	bliog	graphy 69

List of Tables

2.1	Adopted Coefficients
3.1	Vehicle Characteristics
3.2	Scheduled Stops
3.3	Simulated Cases
3.4	Simulation Results - Battery Downsizing
4.1	Asphalt Layer Composition
4.2	Volumetric Composition for Each Pavement Layer
4.3	Material Density
4.4	Asphalt Material in SimaPro
4.5	Machinery Fuel Consumption for Construction
4.6	Machinery Fuel Consumption for Wear Layer Rehabilitation 42
4.7	Machinery Fuel Consumption for Asphalt Refurbishment 43
4.8	Asphalt Construction, Maintenance and Refurbishment Transport . 43
4.9	DWPT Infrastructure Components
4.10	Coil Plate Components
	Energy Delivered
	Asphalt Summary Table
4.13	DWPT Summary Table
4.14	Energy Delivered Summary Table
5.1	Utilisation Ratio
5.2	Total Cost of Ownership
5.3	Initial Baseline Parameter
5.4	TCO Parity
5.5	Government Incentives 64

List of Figures

1.1	Sustainable Development Goals [5]	2
1.2	VECTO structure	3
2.1	BEV traction system	6
2.2	Electric powertrain configurations [11]	7
2.3	Rint circuit [12]	8
2.4	Electrified Road System [15]	9
2.5		10
2.6		11
2.7		12
2.8		12
2.9		14
3.1	Simulation Model Scheme [28]	21
3.2		22
3.3	Mission Profile	23
3.4		25
3.5	eRoad Segments Representation	29
3.6	Simulations Comparison - Presence of eRoad with same battery size	31
3.7	SOC Comparison - Battery Downsizing	32
4.1	Asphalt layers	37
4.2	Total Mass for Each Layer	39
4.3	Dynamic Wireless Power Transfer Infrastructure Layout	44
4.4	Climate Change of Asphalt Materials	48
4.5	Climate Change of Asphalt Construction and Maintenance	49
4.6	Climate Change of Off-Board Charger	50
4.7	Climate Change of Coil plate	51
4.8	Climate Change of On-Board Chargers	52
4.9	Breakdown of Climate Impact for 1 km of ERS	53
4.10	Climate Change and Energy Source Comparison	54

4.11	Comparison of Climate Impact Breakdown between BET and DWPT	56
5.1	TCO for Different Technologies, Utilisation Ratio and Future Scenarios	60
5.2	Purchase Cost Breakdown, year 2022	61
5.3	Energy Carrier Cost Breakdown, year 2022	62

Acronyms

AC Alternate Current

AFIR Alternative Fuels Infrastructure Regulation

BEHDT Battery Electric Heavy-Duty Truck

BET Battery Electric Truck

BEV Battery Electric Vehicle

CPT Capacitive Power Transfer

CU Conductive Unit

CAPEX CAPital EXpenditure

 ${f DWPT}$ Dynamic Wireless Power Transfer

EC Energy Consumption

ECM Equivalent Circuit Model

ECU Electronic Control Unit

EPD Environmental Product Declarations

eRoad Electrified Road

ERS Electrified Road System

FU Funcitonal Unit

GHG Greenhouse Gas

HDV Heavy-Duty Vehicle

HMA Hot-Mix Asphalt

ICE Internal Combustion Engine

IPT Inductive Power Transfer

IRR Internal Rate of Return

LCA Life Cycle Assessment

LCI Life Cycle Inventory

MGPT Magnetic Gear Power Transfer

MTP Microwave Power Transfer

NPV Net Present Value

PCR Product Category Rules

 ${f SDG}$ Sustainable Development Goals

SOC State Of Charge

TCO Total Cost of Ownership

TEN-T Trans-European Transport

UT Utilisation Ratio

VECTO Vehicle Energy Consumption calculation TOol

WPT Wireless Power Transfer

Chapter 1

Introduction

1.1 CO₂ European Legislations for Heavy-Duty Vehicles

In the context of the global effort to combat climate change, the transport sector makes a significant contribution to the Greenhouse Gas (GHG) emissions. This is correlated with its dependency on fossil fuels, which makes decarbonization particularly challenging, especially for road freight transport, responsible for over 6% of the total European GHG emissions [1].

Aligned with the Sustainable Development Goals (SDG) [2], established by the United Nations in 2015 and illustrated in Figure 1.1, and in particular with Goal 13: Climate Action, the European Union has introduced important regulations on CO_2 emissions, extending their scope beyond light-duty vehicles to include HDV as well.

To this end, Regulation 2019/1242 [3] was the first-ever CO_2 emission standard introduced by the European Union. The regulation, released in 2019, set a target reduction of 15% for all HDV manufacturers, specifically for lorries over 16 tonnes. Later, in 2024, the amendments introduced by Regulation 2024/1610 [4] revised the original one. In particular, these amendments cover a wider range of lorries, including medium-duty, city buses, coaches, and trailers. The revised regulation sets new and more ambitious CO_2 emission reduction targets: 45% by 2030, 64% by 2035, and 90% by 2040.



Figure 1.1: Sustainable Development Goals [5]

1.1.1 **VECTO**

To measure and monitor vehicle fuel consumption and CO_2 emissions, both physical tests and simulations are performed. Physical testing is performed only at the component level, such as for the engine, while simulations are carried out using the Vehicle Energy Consumption calculation TOol (VECTO). This tool allows the evaluation of the vehicle's longitudinal dynamics to obtain the desired output, without the need to perform real-world testing, which is not always feasible. The input data include the vehicle class, to extract the standard parameters and the driving cycle, the results of the component test, and, if available, the validation data [6]. Figure 1.2 illustrates a schematic of the VECTO structure.

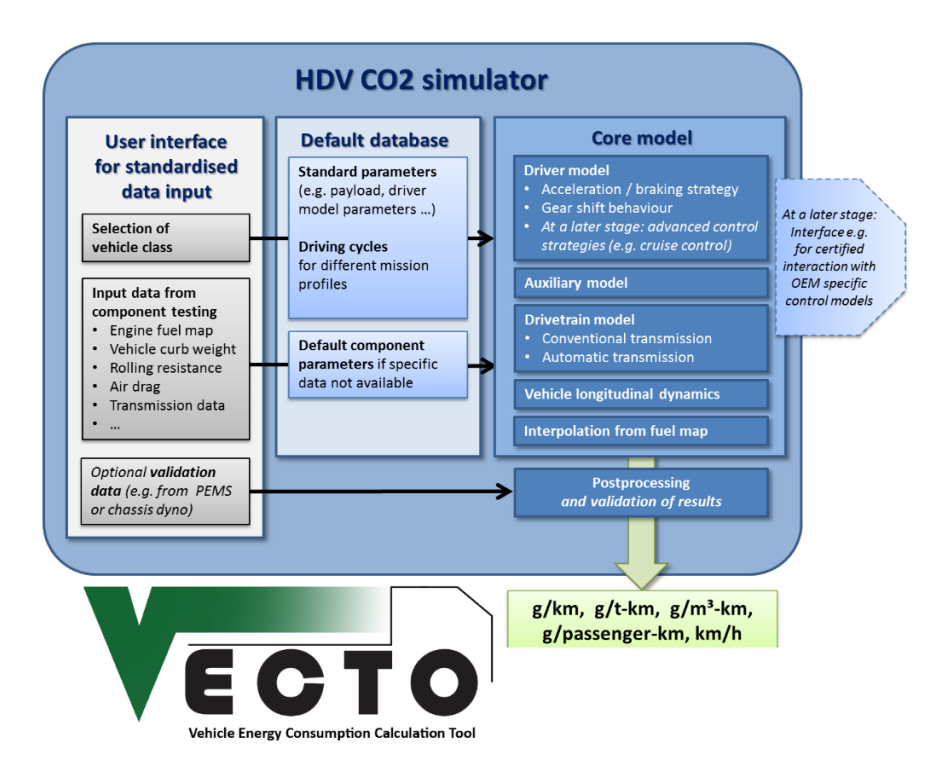


Figure 1.2: VECTO structure

1.2 Aim and Scope of the Thesis

The increasingly stringent European Union regulations on greenhouse gas emissions in the transport sector, particularly for heavy-duty vehicles, require new innovative solutions to reduce the environmental footprint of road freight transport. In this context, Battery Electric Trucks (BET) represent one of the most promising alternatives to conventional diesel trucks. However, three main problems are slowing down their introduction: the limited driving range, the long recharging times required by conventional static charging stations, and the reduction in the allowed transportable payload.

Electrified Road Systems (ERS), which enable dynamic wireless charging while driving, offer a potential answer to these limitations by allowing smaller batteries, increased vehicle range, and reduced stop time. However, the implementation of such an infrastructure raises questions not only regarding its technical feasibility, but also about its environmental and economic sustainability.

The main objective of this thesis is therefore to evaluate both the climate and the economic impacts associated with the deployment of an ERS for highway freight transport. To achieve this goal, two methodologies were adopted: Life Cycle Assessment (LCA), to quantify the environmental impact of the system throughout its lifetime, focusing on the infrastructure impact, and Total Cost of Ownership (TCO), to assess its economic impact, trying to understand if this technology may be economic feasible with respect to BET.

The scope of the thesis encompasses the definition of a representative case study for a long-haul route in Italy, the modelling of the mission profile directly extracted from the real route, the assessment of different utilisation scenarios, and technological configurations.

1.3 Structure of the Thesis

The work is organised as follows:

- Chapter 2 introduces the background concepts and technical aspects necessary to understand the technologies and methodologies analysed throughout the work;
- Chapter 3 presents the case study, including the definition of the reference vehicle and mission profile;
- Chapter 4 describes the Life Cycle Assessment, detailing the life cycle inventory (LCI), the modelling of different scenarios, and the results of the impact assessment;
- Chapter 5 presents the Total Cost of Ownership analysis, comparing the economic implications of deploying an ERS for BET charging compared to the use of static charging stations;
- Chapter 6 summarises the main findings of the thesis, highlighting the implications and possible directions for future research.

Chapter 2

Fundamental Elements of the Thesis

This chapter provides an overview of the four main topics that form the basis of the thesis: Battery Electric Truck (BET), Electrified Road System (ERS), Life Cycle Assessment (LCA), and Total Cost of Ownership (TCO).

2.1 Battery Electric Truck

The recent restrictions introduced by the European legislation (Section 1.1) have increased the pressure on truck manufacturers to innovate vehicle propulsion systems. Particularly, the regulations aim at reducing the greenhouse gas emissions for the heavy-duty sector, traditionally powered by internal combustion engine (ICE). As a consequence, to meet both the environmental and performance requirements, alternative solutions are continuously explored.

Among the different approaches, hybrid powertrains represent an intermediate step, combining a conventional ICE with an electric motor and a battery pack, improving fuel efficiency and reducing emissions [7]. Another promising option is the fuel cell systems. They can be designed either as a pure hydrogen fuel cell system or as a hybrid configuration integrating a battery pack to provide additional power. In both cases, the only direct emission is water vapour, making them a clean solution. Hydrogen-based systems also offer high energy density and rapid refuelling, though challenges remain regarding storage safety and overall system efficiency [8].

Despite the different alternatives, fully electric powertrains are currently considered the most immediate deployable solution. This is due to the increasing maturity of battery technologies, the progressive development of charging infrastructure, compatible with light-duty passenger vehicles and therefore shareable between HDVs and passenger cars, and the relative simplicity of electric drivetrains compared to combustion-based systems. Nevertheless, their large-scale introduction in heavy-duty transport faces limitations due to driving range extension and payload capacity [9].

2.1.1 Basic Electric Powertrain Topologies

The basic concept of a pure electric powertrain is very simple: the energy stored in the battery is converted into mechanical power at the wheels through the inverter, the AC motor, and the transmission system. Instead, during braking, the bidirectional nature of the electric powertrain (i.e., battery system, inverter and AC motor) enables regenerative braking. This configuration is illustrated in Figure 2.1.

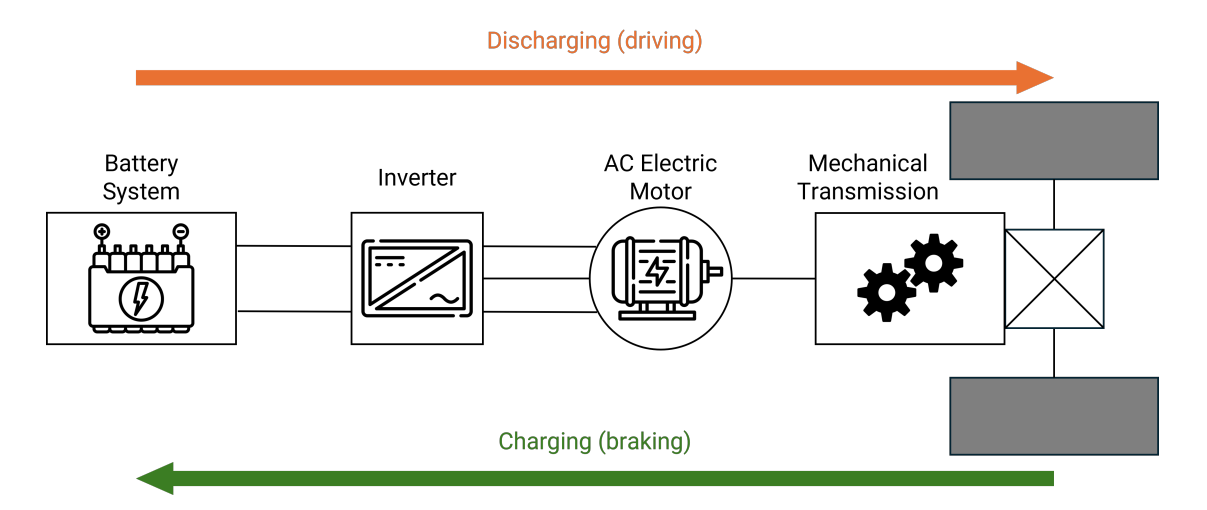


Figure 2.1: BEV traction system

Depending on the arrangement of components, different topologies can be adopted. The three most common solutions are central drive, in-wheel drive, and near-wheel drive [10].

- Central Drive: this configuration (Figure 2.2a) permits to easily replace the ICE with the electrical components, as previously introduced. Although cost-effective, it is unsuitable for HDV applications due to its limited energy efficiency and its volume occupation;
- In-wheel Drive: as the name suggest, in this solution (Figure 2.2b) the electric motor directly powers the wheel. Despite its compactness, this configuration can not be employed in HDV since the operating window is much lower than

the one required. In addition, the in-wheel drive has a high cost and complexity for design and development;

• Near-wheel drive: this configuration (Figure 2.2c) offers a trade-off between efficiency, compactness, and cost, making it the most suitable option for HDV applications.

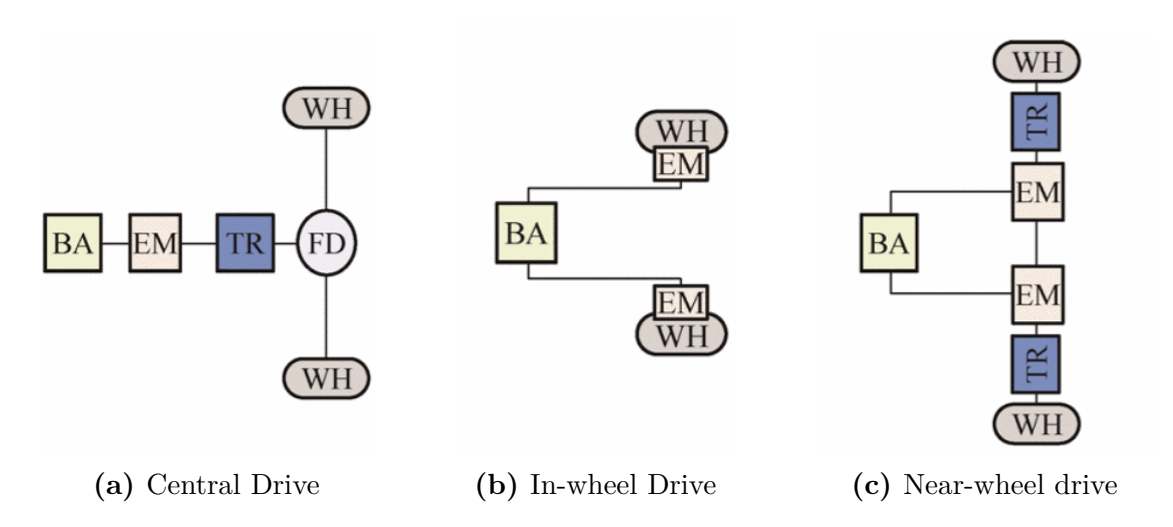


Figure 2.2: Electric powertrain configurations [11]

2.1.2 Battery Equivalent Circuit Model

Accurate modelling of battery behaviour is fundamental to simulate energy flows, especially in electric vehicles. Equivalent Circuit Model (ECM) provides a simplified and effective representation of battery dynamics, enabling efficient calculations of charging processes.

Different ECM types exist in the literature, offering various levels of complexity and accuracy. The most common are:

- Rint model: an ideal voltage source (U_{OCV}) , dependent on the battery SOC, in series with an internal ohmic resistance (R_0) ;
- Thevenin model: extend the Rint model by adding a parallel RC group to consider transient behaviour and voltage relaxation effects;
- Dual Polarisation model: includes two RC groups, improving accuracy at the expense of complexity.

In this thesis, the *Rint* model is adopted due to its simplicity and computational efficiency. Although it does not capture dynamic or thermal phenomena, it is

sufficient for estimating steady-state charging power and current [12]. The model is shown in Figure 2.3.

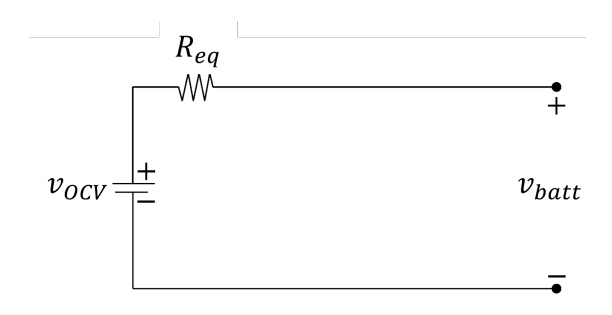


Figure 2.3: Rint circuit [12]

The charging current can be derived from a power balance equation. The power delivered to the battery (P_b) , considering inverter losses and other system inefficiencies, is expressed as:

$$Pb = v_b \cdot i_b = (v_{ocv} - R_{eq} \cdot i_b) \cdot i_b \to R_{eq} \cdot i_b^2 - v_{ocv} \cdot i_b + P_b = 0$$
 (2.1)

This quadratic equation relates the input power to the battery with the resulting current and voltage drop. Its solution provides the current flowing into the battery (i_b) :

$$i_b = \frac{v_{OCV} - \sqrt{v_{ocv}^2 - 4 \cdot P_b \cdot R_{eq}}}{2 \cdot R_{eq}}$$
(2.2)

In Equation 2.2, the negative root is taken since the charging phase is considered, where the current flows into the battery.

2.2 Electrified Road System

Electrified Road System (ERS) has, for several years now, been one of the technologies aimed at reducing the environmental impact of the transport sector. In particular, ERS reduces carbon emissions and reliance on fossil fuel [13]. Furthermore, it enables dynamic charging of vehicles while travelling, thereby reducing the need to stop for recharging and mitigating drivers' range anxiety.

An ERS is composed of six subsystems [14, 15], illustrated in Figure 2.4:

• Energy Subsystems: includes elements for the generation, transmission, distribution, and management of electricity supplied to the Power Transfer Subsystem;

- Road Subsystem: consists of barriers, pavements, and auxiliary components to ensure safe traffic conditions;
- Power Transfer Subsystem: enables energy transfer from the *Energy* to the *Vehicle Subsystem*, through both road-embedded and on-board components, including control units;
- Vehicle Subsystem: comprises devices that convert the received energy into propulsion or storage in the battery;
- Payment and Access Subsystem: located on-board, it manages user authentication, activation and payment of the Power Transfer Subsystem, depending on location and time of use;
- Safety and Control Subsystem: continuously monitors the system and manages any safety-related issues associated with the eRoad.

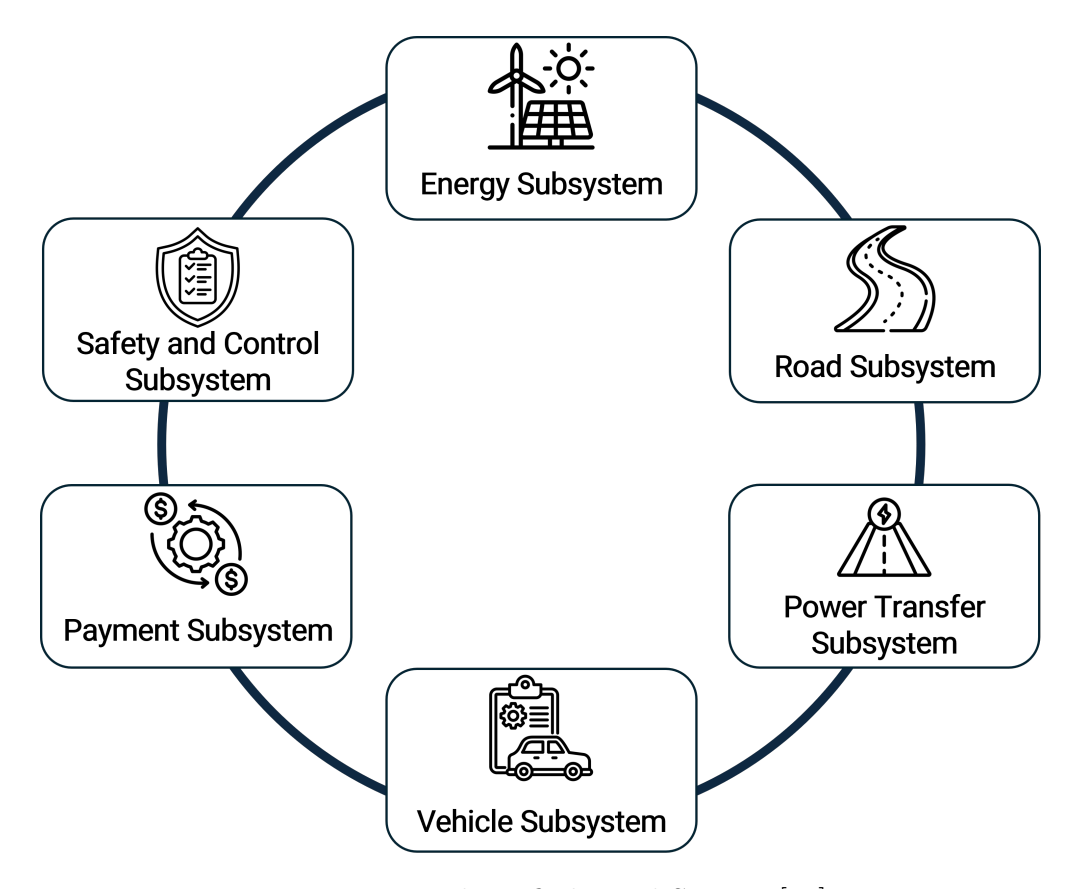


Figure 2.4: Electrified Road System [15]

ERS solutions are typically classified according to their power transfer method into two categories: contact charging systems and contactless (wireless) charging systems [15].

2.2.1 Contact Charging

As the name suggests, the contact-based solutions require a physical connection between the road infrastructure and the vehicle. Two main solutions can be distinguished depending on the location of the conductive elements.

Overhead Solution

The overhead system (Figure 2.5) consists of conductive wires to establish continuous direct contact between the power supply and the vehicle. The system is composed of two groups of components: on-board devices and roadside infrastructure [16]. The former includes the pantograph, the control electronics, and the electric powertrain, while the latter comprises all the electrical distribution systems.

This solution is primarily suited for heavy-duty trucks and buses, since, for safety reasons, the minimum distance of the power supply is set at 5 meters [17].

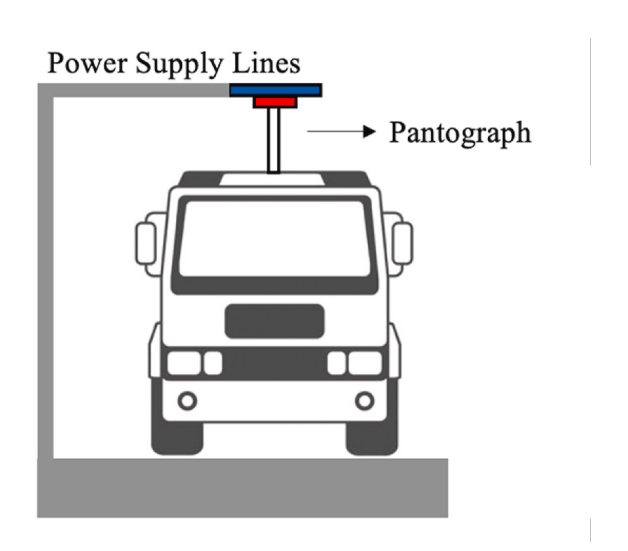


Figure 2.5: Overhead Solution [18]

Conductive Rail Solution

The working principle of the conductive rail system is very similar to the overhead solution. The difference is in the conductor type: in this case, the vehicle is charged through rails embedded in, or mounted on, the road surface. Once aligned with the rails, the vehicle lowers a mechanical arm to establish the connection [15] (Figure

2.6a). Alternatively, the rails may be positioned roadside (Figure 2.6b). There are three main elements composing the systems [16]: in-road infrastructure (rail, cables, drainage), on-board devices, and roadside equipment.

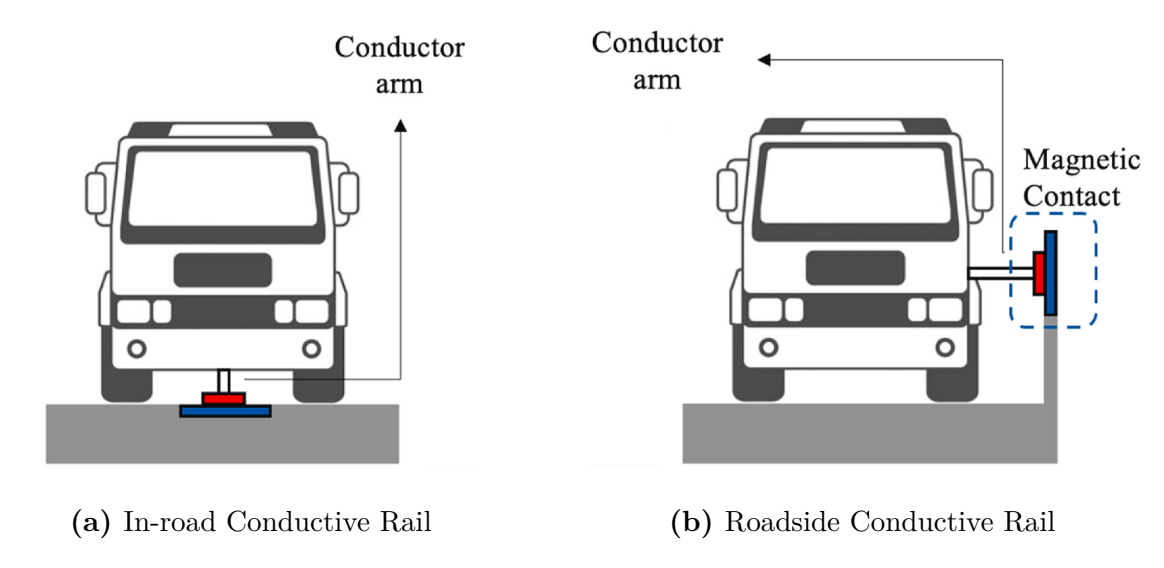


Figure 2.6: Conductive Rail Solutions [18]

2.2.2 Dynamic Wireless Power Transfer

DWPT technology represents a contactless alternative for dynamic charging applications. Several methods have been proposed, including Microwave Power Transfer (MTP), Capacitive Power Transfer (CPT), and Magnetic Gear Power Transfer (MGPT). However, the most widely studied and applied solution is Inductive Power Transfer (IPT).

Inductive Power Transfer Solution

IPT uses an electromagnetic field to transfer the power from one coil (primary) embedded in the pavement to the receiver coil (secondary) installed on the vehicle without any physical connection between the two. This principle is based on Faraday's Law, according to which a current in one circuit induces a voltage across another, creating a time-varying magnetic field [19], as illustrated in Figure 2.7.

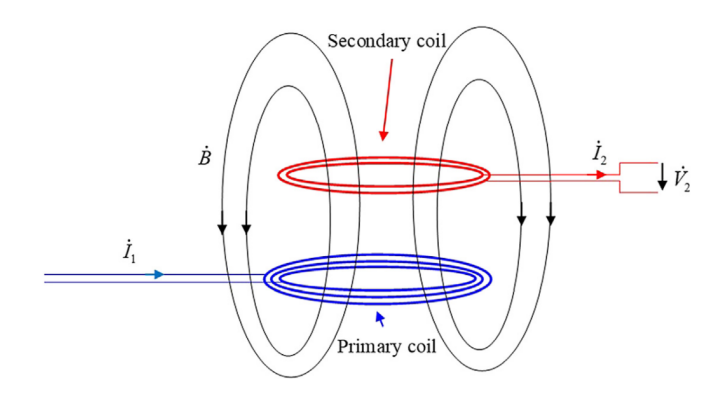
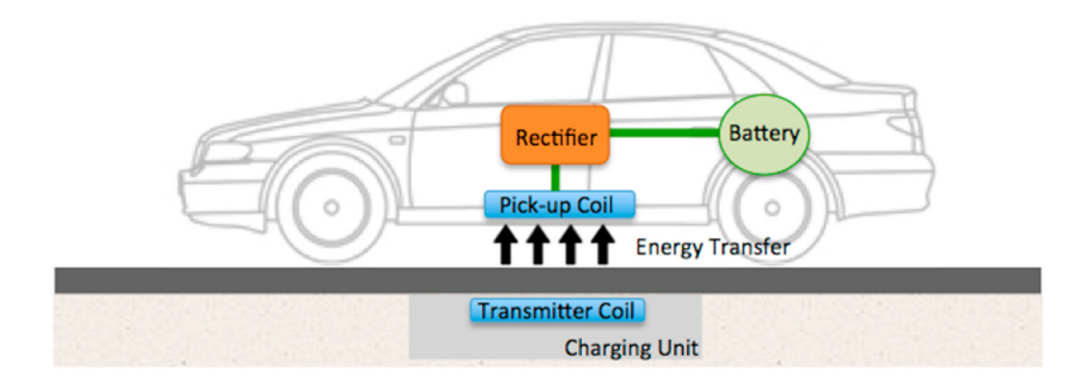
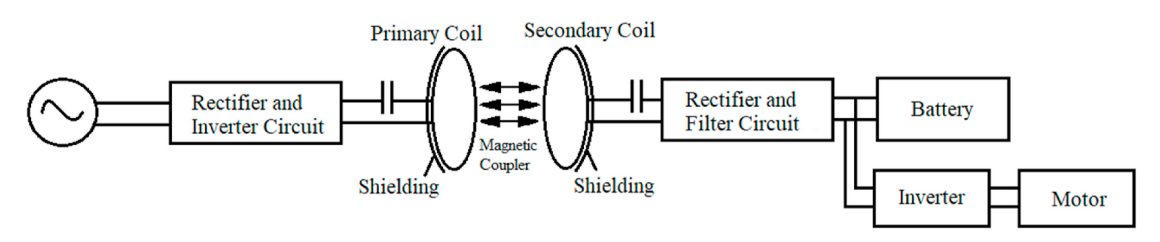


Figure 2.7: Two Coupled Coils [19]

Therefore, when alternating current is supplied to the transmitter coil, an alternating magnetic field is generated. As the vehicle passes over the electrified road, the magnetic flux induces a current in the receiving coil. On-board rectifiers then convert this alternating current into direct current, which is used to charge the battery and drives the motor [15]. An example of the system is shown in Figure 2.8a, with a schematic representation provided in Figure 2.8b.



(a) Illustration of IPT



(b) IPT Schematic diagram

Figure 2.8: IPT solution [18]

2.3 Life Cycle Assessment

The Life Cycle Assessment (LCA) is a methodology to quantify the environmental impact of a product or service during its entire life cycle, from raw material extraction to end-of-life disposal or reuse [20].

LCA is standardised by two ISO norms:

- ISO 14040:2021 [21], which defines principles and frameworks;
- ISO 14044:2021 [22], which specifies the requirements and guidelines.

Based on these standards, ISO 14025:2010 [23] introduces the concept of Product Category Rules (PCR) and Environmental Product Declarations (EPD). The former establishes common rules for calculating the environmental impacts of products within the same category, while the latter represents a standardised document that companies can publish to communicate the environmental profile of a product.

According to ISO guidelines, an LCA study consists of four main phases [24]:

- 1. Goal and Scope definition: definition of the product to be analysed and the objective of the study. This phase also requires the specification of the Functional Unit (FU) and the identification of the system boundaries, for example, which life cycle stages are included or excluded from the analysis;
- 2. Life Cycle Inventory (LCI): the most time-consuming phase, involving the collection and quantification of all relevant input and output flows associated with the product;
- 3. **Impact Assessment**: calculation of the potential environmental impacts through the selected impact categories and assessment methods;
- 4. **Interpretation**: critical analysis of the results obtained in the previous steps, aimed at making conclusions.

With reference to the system boundaries defined in the first phase, the product life cycle is typically divided into five stages: raw material extraction, production, transportation, use, and end-of-life. Depending on which stages are included, different life cycle models can be applied (Figure 2.9):

- the *Cradle-to-Gate* model excludes use and end-of-life stages, focusing only on processes up to the product distribution phase;
- the *Cradle-to-Grave* model includes all five stages, from raw material extraction to final disposal;

• the *Cradle-to-Cradle* model, similar to *Cradle-to-Grave*, replaces the waste stage with recycling or reuse, thus closing the loop and promoting circularity.



Figure 2.9: Product Life Cycle and Models

2.4 Total Cost of Ownership

The Total Cost of Ownership (TCO) is a methodology used to evaluate the economic impact of an asset or service over its entire lifecycle, taking into account both direct and indirect costs [25]. The analysis goes beyond the initial purchase cost and also includes the maintenance expenses, operating costs related to the energy carrier, driver costs, and additional taxes and fees. Moreover, the TCO considers the residual value of the asset, which is its estimated worth at the end of its service life after depreciation [26].

The TCO is evaluated through the Net Present Value (NPV), which represents the present value of the expected future cash flows, both positive and negative, over

the entire lifecycle and discounted to the present [27]. It is evaluated as:

$$NPV = \sum_{t=0}^{T} \frac{CF_t}{(1+r)^t}$$
 (2.3)

where CF_t is the present value of the expected cash flow during the period t, r is the discount rate, and T is the total number of periods.

In the following sections, each cost component considered in the TCO analysis is described in detail, taking as reference the article published by Costantino et al. [28].

2.4.1 Purchase Cost

Since no data were available regarding the purchase cost of BET and BET equipped with DWPT, an estimation was performed starting from the price of a Group 5 VECTO truck propelled by an internal combustion engine. In particular, the initial purchase cost was set equal to €170000 [28]. A distinction was then made between subsystems common to both technologies, while components not shared were removed and replaced with those required for the zero-emission configurations.

2.4.2 Maintenance Cost

The maintenance cost for BET and BET equipped with DWPT includes only repair and preventive maintenance, as well as tyre replacement for driven, non-driven, and trailer wheels. It is important to point out that, due to the absence of the internal combustion engine, lubricant oil changes and AdBlue refilling are not considered.

2.4.3 Driver Cost

The driver cost includes the average salary, travel allowances, and the employer's social contributions.

According to the Comité National Routier [29], the total annual driver cost for Italy amounts to €57246, corresponding to an hourly rate of €30.78.

2.4.4 Taxes and Fees

According to the European Commission report [30], transport-related taxes in Italy include a registration tax equal to $\in 1500$, an annual ownership tax of $\in 1000$, and yearly insurance expenses of $\in 3000$.

Additionally, highway toll fees were considered equal to $\leq 0.19/km$, as reported by ICCT [31].

Energy Carrier Cost 2.4.5

A crucial component of the TCO is the cost related to energy consumption for battery charging.

For the case under study, three charging technologies were considered: fast charging (at 350 kW), slow charging at the depot (100 kW) and dynamic charging through the eRoad.

The model used to evaluate the cost first involves the evaluation of the net cash flow (CF_n) , required to ensure a viable investment for the infrastructure owner. It is defined considering the initial capital expenditure (CAPEX) and the desired internal rate of return (IRR):

$$CF_n = \frac{CAPEX}{\sum_{t=1}^{T} \frac{1}{(1+IRR)^t}}$$
 (2.4)

In addition, the ERS tariff, representing the cost per unit of energy consumed, is evaluated as the ratio between the minimum revenue that must be generated to cover costs and achieve profitability, and the annual energy sold:

$$ERS \ Tariff = \frac{R}{ES_u} \tag{2.5}$$

The revenue is computed as:

$$R = CF_n + E_u \cdot OPEX_{kWh} + M \tag{2.6}$$

Where E_y is the annual energy consumption cost, $OPEX_{kWh}$ corresponds to the operating expenses per kilowatt-hour, and M is the annual maintenance cost. The annual energy terms are defined as:

$$E_y = \frac{P \cdot (UT \cdot W_y \cdot h_d)}{\eta} \qquad (2.7) \qquad ES_y = P \cdot (UT \cdot W_y \cdot h_d) \qquad (2.8)$$
 With the following parameters:

- P: maximum deliverable power by the ERS;
- UT: utilisation ratio, corresponding to the number of trucks per day using the eRoad;
- W_{u} : number of working days per year;
- h_d : average number of operating hours per day;
- η : on-board charger efficiency.

2.4.6 Residual Value

The residual value (RV) is an important component of the TCO analysis, as it represents the remaining value of an asset at the end of its operational life after depreciation.

The residual value of the truck is determined by accounting for the depreciation of both the vehicle body and the battery pack, as expressed by:

$$RV = (C_v - C_b) \cdot expA_v^a \cdot expM^m + C_b \cdot expA_b^a \cdot expM^m$$
 (2.9)

Where C_v and C_b are the purchase cost of the vehicle and the battery, respectively, $expA_{v,b}$ and expM are the annual and mileage-related depreciation factors, whose values are reported in Table 2.1 and a and m represent the vehicle age (expressed in years) and the mileage (expressed in thousands of kilometres) [28].

Table 2.1: Adopted Coefficients

Coefficient	Value
$expA_v$	0.922
$expA_b$	0.968
expM	0.999

Chapter 3

Case Study

This chapter presents the case study adopted for the implementation and evaluation of the ERS. The objective is to assess the feasibility of integrating dynamic charging infrastructure in a realistic long-haul freight transport scenario.

The analysis focuses on a battery electric heavy-duty truck (BEHDT) belonging to VECTO Group 5 (5-LH), operating in a highway scenario. This vehicle category, which includes long-haul tractor-trailers, is representative of a large share of freight transport activities across Europe. Indeed, ICCT Report reveals that this vehicle group accounted for 75% of all HDV sales covered under the scope of the CO_2 standards in 2023 [32]. In addition, ACEA reports that subgroup 5-LH accounts for 68.2% of the CO_2 emissions of the entire fleet of analysed vehicles [33].

The selected route connects two major logistics hubs: the Amazon facility in Torrazza, Piedmont, and the Amazon FCO 2 facility in Colleferro, Lazio. The total length of the journey is approximately 715 km, corresponding to a typical long-haul mission profile for heavy-duty trucks.

3.1 Vehicle Characteristics

As introduced above, the vehicle under consideration is a long-haul BEHDT belonging to VECTO Group 5. It is modelled as a 4×2^{-1} tractor unit with a gross vehicle mass (GVM) of 40 tons, which is a typical configuration for European long-distance freight transport.

The reference truck for the analysis, similarly to the market-available BET [34, 35], is equipped with a battery pack delivering a nominal energy of 700 kWh and, in

¹The vehicle has four wheels in total, but only two of those are driven by the engine power

case of ERS engaged, an on-board charger of $80 \ kW$. These configurations were selected as the base scenarios to assess the:

- Comparison between BET and BET with the adoption of DWPT in terms of energy consumption and state of charge (SOC) profile;
- Reduction in delivery time to complete the mission;
- Possibility of performing battery downsizing combined with an increased on-board charger power in favour of weight reduction.

Table 3.1 reports the main vehicle specifications adopted in the simulations, including truck mass and aerodynamic, transmission and powertrain details, and battery and charger characteristics.

Component Parameter Value Unit Chassis Mass 15.7 tons Truck Gross Mass 40 tons 5.3 m^3 Drag Area AC_x Speed Ratio 2.59 Final Drive Efficiency Torque-Losses Map $(f(\omega_{input}, T_{input}))$ 3.86 Speed Ratios 1.93 Gear Box Torque-Losses Map $(f(\omega_{input}, T_{input}))$ Efficiency kW Rated Power 125 E-Motor Maximum Torque 1455 NmChemistry NMC Mass 3.9 tons Standard Battery Nominal Energy 700 kWh Nominal Capacity 1000 Ah Mass 100 kg Standard On-Board Charger Rated Power 80 kWEfficiency 80 %

Table 3.1: Vehicle Characteristics

3.2 Simulation Model

To evaluate the truck performance under different infrastructure and battery configurations, a simulation model was developed, following the approach proposed by Costantino et al. [28].

The simulation model adopts a distance-based approach, allowing the introduction of ERS segments within the route while preserving the overall mission length.

The mission profile, comprising road grade, target speed, and resting stops, serves as the main input. A driver model applies a look-ahead approach to anticipate upcoming stops and adjust acceleration or braking accordingly, while respecting powertrain constraints.

The following step involves the handling of longitudinal dynamics, which evaluates the required traction force (F_{veh}) as a function of the vehicle speed (v_{veh}) and road grade (α) :

$$\begin{cases}
F_{veh} = F_{roll} + F_{grade} + F_{aero} + m_{veh} \cdot a_{veh} \\
F_{roll} = (f_0 + f_1 \cdot v_{veh}) \cdot m_{veh} \cdot g \cdot \cos(\alpha) \\
F_{grade} = m_{veh} \cdot g \cdot \sin(\alpha) \\
F_{aero} = \frac{1}{2} \cdot \rho_{air} \cdot AC_x(v_{veh}) \cdot v_{veh}^2
\end{cases}$$
(3.1)

Where f_0 and f_1 are the rolling coefficients, and AC_x is a function of vehicle speed, as wind correction is considered.

Based on the longitudinal dynamic, the electric motor speed (ω_{em}) and torque (T_{em}) are evaluated as:

$$\begin{cases}
\omega_{em} = \frac{v_{veh} \cdot \tau_{fd} \cdot \tau_{gb}}{r_w} \\
T_{em} = \frac{F_{veh} \cdot r_w}{\tau_{fd} \cdot \tau_{gb}}
\end{cases}$$
(3.2)

Here, τ_{fd} and τ_{gb} are the final drive and gear box ratio, respectively, and r_w is the wheel radius.

Finally, once the power coming from the e-motor is evaluated, it is used as input for calculating the battery current (Equation 2.2) and SOC.

The complete simulation model is shown in Figure 3.1.

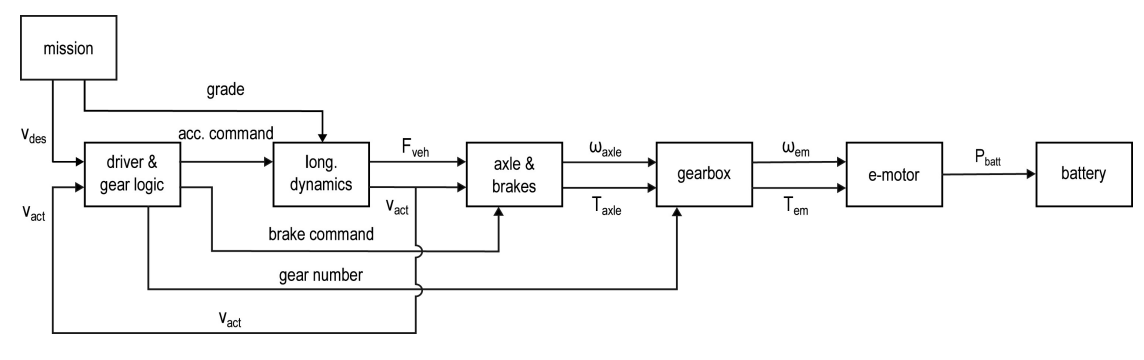


Figure 3.1: Simulation Model Scheme [28]

3.3 Mission Profile

The mission profile was constructed from the GPX track of the selected route, downloaded using GraphHopper Maps [36]. The GPX file contains geographical information, including latitude, longitude, and elevation, which were processed in *MATLAB* [37] using the gpxread function.

Two main graphical representations were obtained:

- A GPS map showing the route, highlighting the key locations along the path such as the start, the two important highway toll booths Milano Ghisolfa and Melegnano, the stops' location for recharging, divided between mandatory and not, and the destination Colleferro. The stops will be deeply described in the following section;
- An elevation profile plotted against the distance, which shows the topographical variation through the mission.

The result is shown in Figure 3.2.

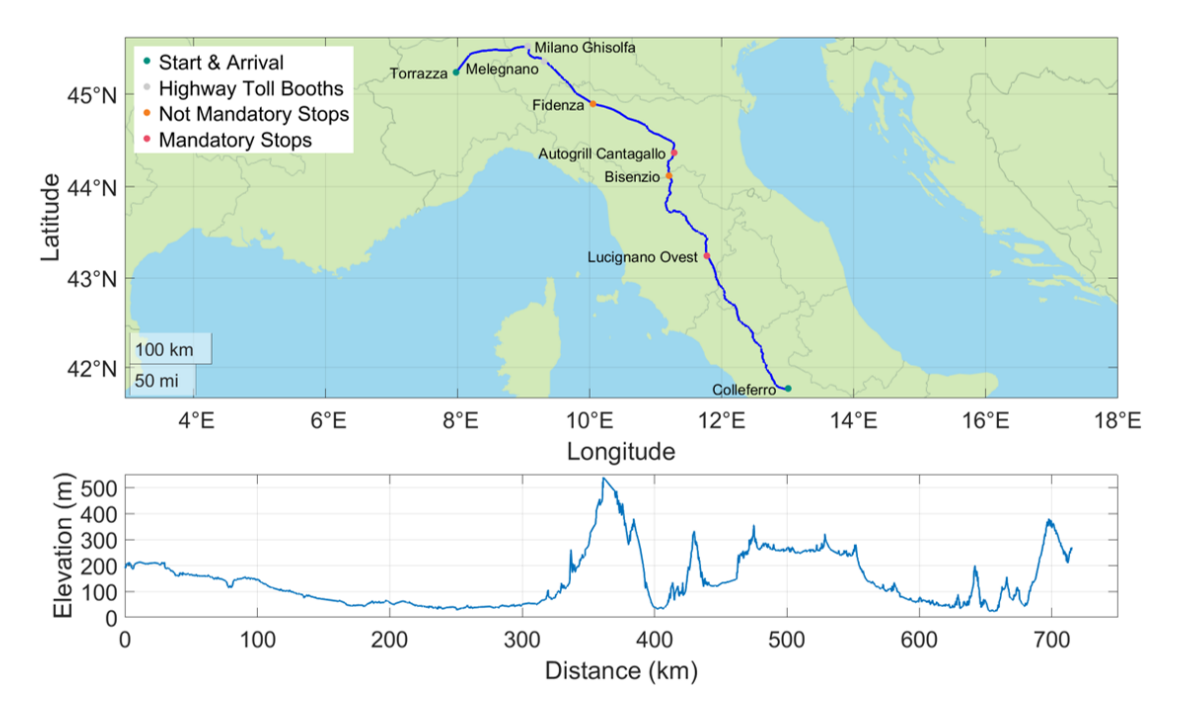


Figure 3.2: GPS route map & Elevation vs Distance

3.3.1 Road Grade

To evaluate the road grade along the mission, a simple equation was adopted:

Grade (%) =
$$\frac{\Delta Elevation \ (m)}{\Delta Distance \ (m)} \cdot 100$$
 (3.3)

The values were constrained within \pm 6 % to avoid unrealistic peaks and interpolated over the distance vector to obtain a continuous profile.

3.3.2 Speed Profile

The speed profile was generated from the "Average Speed" data provided by Graph-Hopper, considering the legal HDV limit of $80 \ km/h$ [38]. Finally, the data were interpolated with a uniformly spaced distance vector.

Figure 3.3 shows both the speed and road grade profile. Additionally, vertical lines are introduced corresponding to the stops' location for recharging.

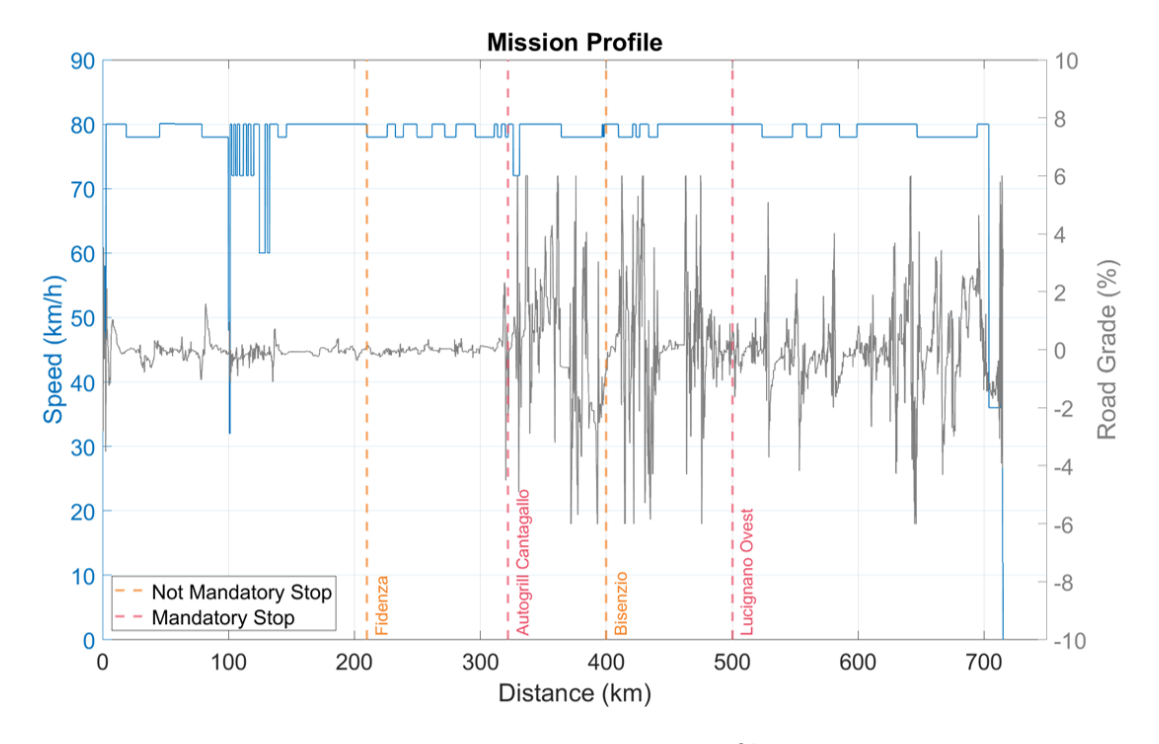


Figure 3.3: Mission Profile

It is important to highlight that the speed profile is not lowered to zero when a stop is detected because of the logic implemented for battery charging, described in the following.

3.3.3 Stops

Schedule stops were introduced to account for mandatory rest breaks and potential charging needs.

Driving regulations limit daily driving to 9 hours, with mandatory 45-minute breaks every 4.5 hours of continuous driving [39]. For this reason, stops were classified as mandatory or optional, each characterised by location, duration and charging power.

Table 3.2 summarises the adopted schedule.

Stops	Distance	Duration	Mandatory	Charging Power
этора	(km)	(s)	(-)	(kWh)
1	0	2	1	0
2	210	1800	0	350
3	322	2700	1	350
4	400	3600	0	350
5	500	2700	1	350
6	715.144	2	1	0

Table 3.2: Scheduled Stops

The binary variable in the "Mandatory" field indicates if a stop is compulsory. Specifically, the stops at $322 \ km$ and $500 \ km$, corresponding to service areas of "Cantagallo" (BO) and "Lucignano Ovest" (AR), are mandatory due to the legal driving time limits. The other two non-mandatory stops are located near Fidenza and Bisenzio. In addition, two technical stops, placed at the start and end of the mission, are included for simulation initialisation and termination purposes.

The location of the stops follows the requirements established by the Alternative Fuels Infrastructure Regulation (AFIR), which sets the installation of fast charging stations with a power of 350 kW for BET every 60 km along the Trans-European Transport (TEN-T) core network, and every 100 km along the more extensive comprehensive corridor starting from 2025, with a complete network coverage expected by 2030 [40].

3.4 Battery Charging During Stops

Once the mission profile was clearly defined, the simulation of the truck began taking into account two distinct scenarios: the first considering the presence of the electrified road along the route, and the second excluding it. This permits a more comprehensive analysis of the truck's behaviour under different infrastructure

conditions.

Among the various elements considered during the simulation, the study mainly focuses on the battery charging phase during scheduled stops.

As described in subsection 2.1.2, the *Rint* equivalent circuit was adopted to simplify the modelling of the battery charging phase.

The main condition that determines whether the truck needs to stop, when not mandatory, is the current battery State of Charge (SOC). The control logic was designed to ensure that the truck maintains a sufficient energy level at all times to complete the planned mission successfully. Indeed, the objective of this strategy is to minimise range anxiety. To achieve this, a SOC-threshold methodology was implemented, considering the charging infrastructures available.

Specifically, when the truck is travelling on a highway segment equipped with an eRoad, and the SOC drops below 30%, the vehicle must stop for recharging at $350 \ kW$. Conversely, in the absence of the eRoad, the threshold that triggers a stop is increased to 40%. This difference in the SOC threshold reflects the opportunity to recharge the battery while driving on the eRoad, justifying a slightly lower battery level. The logic scheme is reported in Figure 3.4.

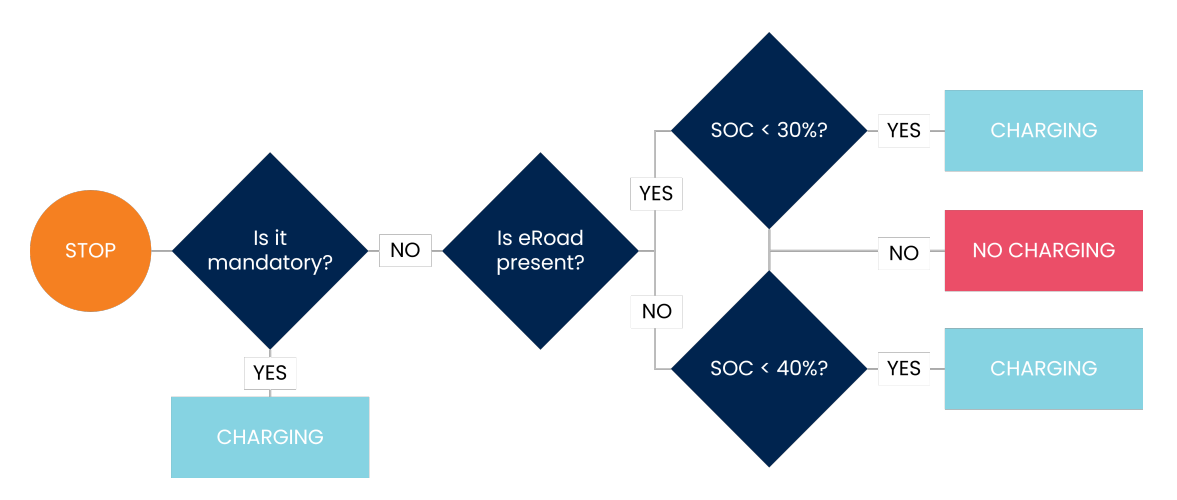


Figure 3.4: Charging logic scheme

It is also worth noting that, if the simulation detects that the conditions for a recharge stop are met, the speed profile is automatically adjusted. In particular, it is reduced to zero to simulate the stop of the truck.

Below, the function chargingStopsNeeded created is reported.

```
function [veh, prof, inCharging] =
     chargingStopsNeeded(driver, veh, missionData, prof, dyn,
     inCharging)
      %Recharge the battery if necessary during the expected
2
      %inCharging becomes true until the stop duration is not
3
       complete
      isChargingStop = driver.state == "stop" &&
5
      driver.stop_time ~=
6
     missionData.stops.duration(driver.nextStop) ...
      && missionData.stops.duration(driver.nextStop) > 10;
      if missionData.stops.mandatory(driver.nextStop)
          % Mandatory Stop
10
          if isChargingStop
              inCharging = true;
12
               [prof, veh] =
13
               chargingBatt(missionData, veh, prof);
          else
              inCharging = false;
          end
      else
18
          % Not Mandatory Stop
          if dyn.eRoad ~= 0 && (prof.battSOC < 0.30 ||
20
                  inCharging)
              % Charging if eRoad present
              if isChargingStop
                   inCharging = true;
                   [prof, veh] =
                   chargingBatt(missionData, veh, prof);
                   inCharging = false;
              end
27
          elseif dyn.eRoad == 0 && (prof.battSOC < 0.40 ||</pre>
28
                  inCharging)
              % Charging if eRoad not present
29
              if isChargingStop
30
                   inCharging = true;
                   [prof, veh] =
                   chargingBatt(missionData, veh, prof);
              else
                   inCharging = false;
34
```

```
end
           else
36
                inCharging = false;
37
           end
38
      end
39
40
      %
41
      function [prof, veh]
42
                   chargingBatt(missionData, veh, prof)
           % Calculate battery current and update SOC
4.3
           pwrCharge =
44
               -missionData.stops.chargingPwr(driver.nextStop);
45
           etaCharge = 0.95;
46
           Pb = pwrCharge * etaCharge;
47
48
           U = veh.batt.ocVolt(veh.x{2});
49
           R = veh.batt.eqRes(veh.x{2});
50
51
           iBatt = (U - sqrt(U^2 - 4*Pb*R)) / (2*R);
           iBatt = real(iBatt);
           iBatt = max(iBatt, veh.batt.minCurr);
           prof.battCurr = iBatt;
56
           veh.x{2} = veh.x{2} - iBatt * veh.dt /
57
              (veh.batt.nomCap * 3600);
           if veh.x\{2\} > 1
59
               veh.x{2} = 1;
60
               prof.battCurr = 0;
61
           end
62
      end
63
  end
```

Listing 3.1: MATLAB Charging Stop Needed

3.5 Slow Battery Charging

Once the truck completed the mission, an additional charging phase at lower power (100~kW) was introduced to restore the battery SOC to 100%. This operation simulates overnight depot charging, typically performed during the driver's rest period. The procedure was implemented through a MATLAB code, which, starting from the SOC at the end of the mission, evaluates the new SOC and the total

energy supplied to the battery. The code accounts for the rated charging power, its charging efficiency, and the maximum available recharging time (8 hours). Furthermore, the code ensures that the charging process is terminated as soon as the SOC reaches 100%, avoiding overestimation of the supplied energy.

```
function [soc, battPrf, E_cons, timeFullCharged] =
     slowCharging(SOC, chPwr, chEff, veh, time)
      battPwr = - (chPwr * chEff);
3
      dt = linspace(1, time, time);
      SOC(1) = SOC;
      for n = 1:length(dt)
9
10
           [soc_new, battCurr(n), battUnfeas(n), battPrf(n)] =
     veh.batt.eval(SOC(n), battPwr, 1);
12
          power_cons_slow(n) =
13
     battCurr(n)*battPrf(n).battOCVolt;
          SOC(n+1) = soc_new;
16
          if battUnfeas(n)
               break;
          end
20
          timeFullCharged = n/3600; %hour
      end
23
      soc = soc_new;
24
25
      battPrf = battPrf;
26
27
      E_cons = abs(trapz(veh.dt,power_cons_slow)); %(J)
28
 end
29
```

Listing 3.2: MATLAB Slow Charging

3.6 Simulation Results

In this section, the results obtained by the simulation are presented.

As a first step, the electrified road segments were defined. As established by Akbari et al. [41], the percentage between 30% and 40% of the total roadway length is considered suitable for electrification. Based on this, a total of 200 km of eRoad was implemented in the study, corresponding to approximately 30% of the route. These electrified sections were introduced in the mission profile as four segments of 50 km each, distributed along the route as illustrated in Figure 3.5.

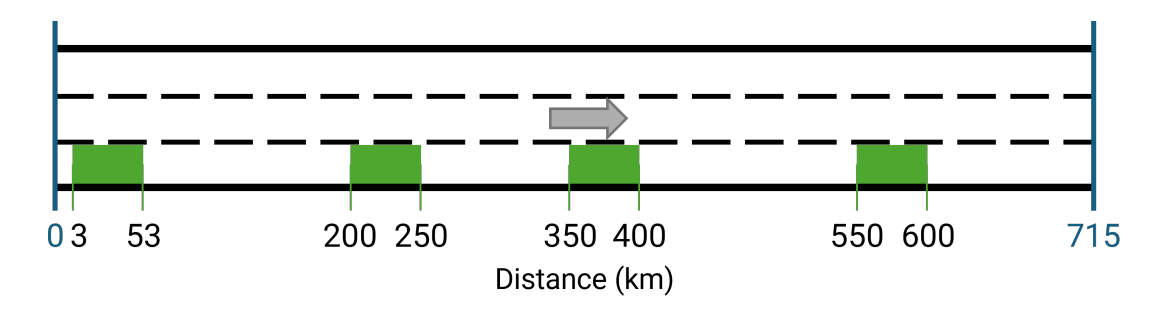


Figure 3.5: eRoad Segments Representation

The cases analysed both with empty and loaded trucks are summarised in Table 3.3.

Presence of eRoad	Battery size	On-Board Charger Power
Tresence or croad	(kWh)	(kW)
No	700	-
	700	80
Yes	475	80
	400	120
	375	160

Table 3.3: Simulated Cases

3.6.1 Correct Functioning of the Simulation

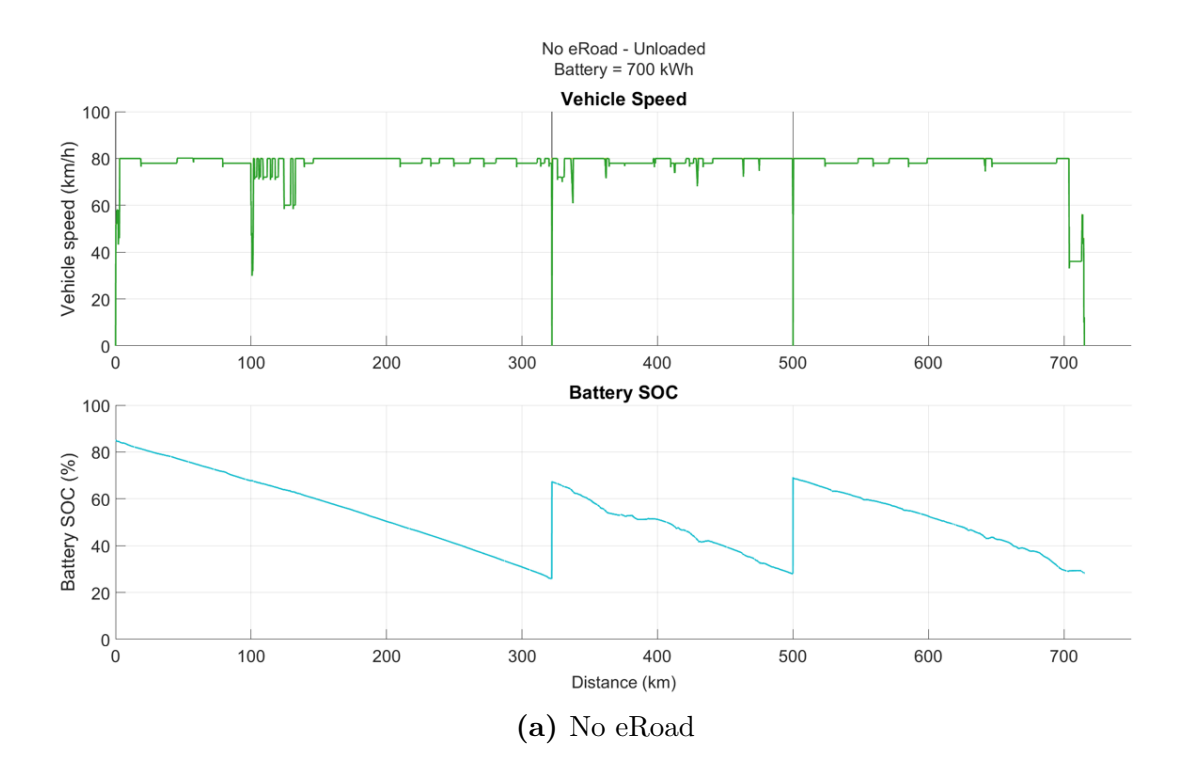
The first analysis, aimed at verifying the correct functioning of the simulation and assessing any potential reduction in delivery time, focused on comparing the simulated truck behaviour during the entire mission with and without the presence of the eRoad, assuming the same battery capacity of $700 \ kWh$.

For the sake of simplicity, the two simulation results reported in Figure 3.6 refer to the case of an empty truck.

In addition, it is important to note that, in all simulation results, the slow charging phase is not included in order to focus only on the truck's dynamic behaviour during the driving mission.

As can be observed, the introduction of the eRoad enables dynamic battery charging, resulting in a final SOC level higher than the one obtained without eRoad. In both cases, the vehicle performs the two mandatory stops and completes the mission without requiring additional charging stops. Consequently, the total mission time remains unchanged, meaning that the eRoad does not lead to a reduction in delivery time for this route.

It is also worth noting that, when travelling along the eRoad segments, the vehicle speed profile is adjusted to the operating speed of $80 \ km/h$.



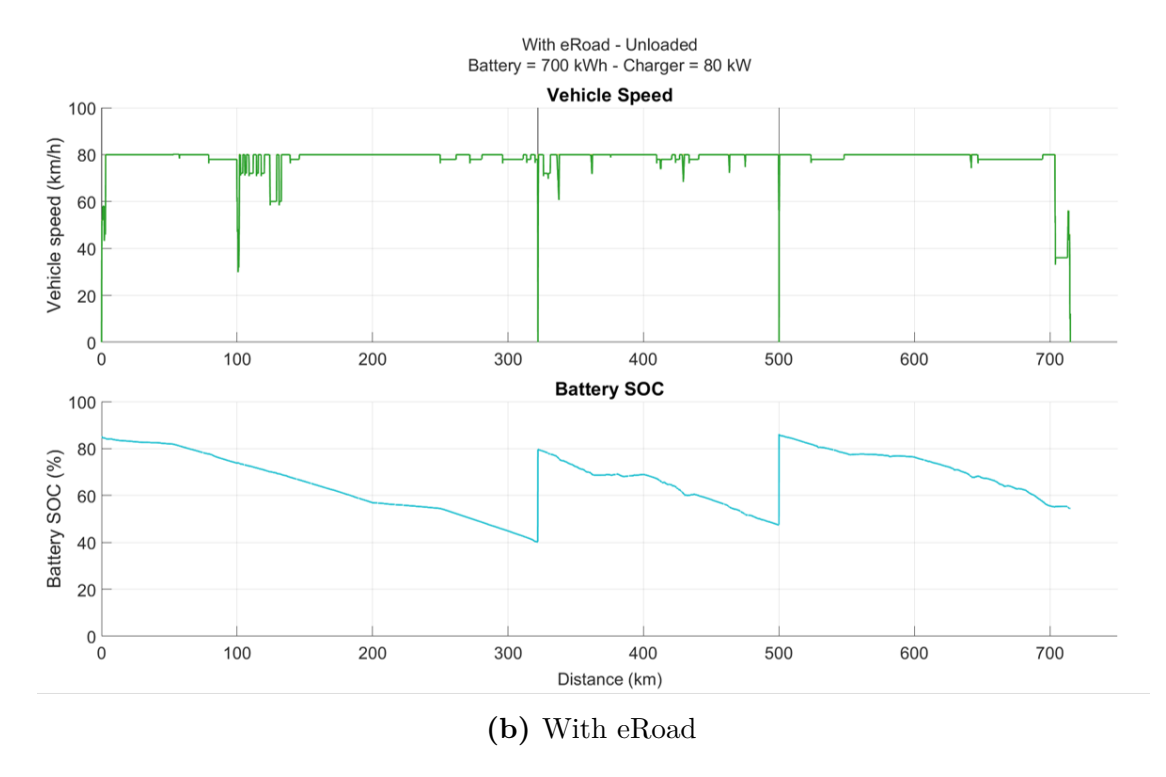


Figure 3.6: Simulations Comparison - Presence of eRoad with same battery size

The overall energy consumption, calculated as the energy delivered by the battery, was 1.166 kWh/km without the eRoad, and 1.181 kWh/km when the eRoad was included, considering that the energy supplied by the ERS was 0.224 kWh/km.

3.6.2 Battery Downsizing

The initial comparative analysis, which showed that implementing the ERS did not significantly reduce the delivery time for a truck with a standard battery capacity, motivated the subsequent focus on the ERS's primary benefit: battery downsizing. As detailed in Table 3.3, the battery capacity was progressively reduced by approximately 32%, 43%, and up to 46% compared to the baseline configuration, accompanied by a necessary increase in the on-board charger power. This power increase is essential for maximising energy recovery in the non-electrified segments, thereby mitigating the risk of deep discharging associated with smaller battery packs.

Figure 3.7 compares the SOC profiles obtained with the different configurations of battery capacity and on-board charger power, considering both unloaded and loaded truck scenarios.

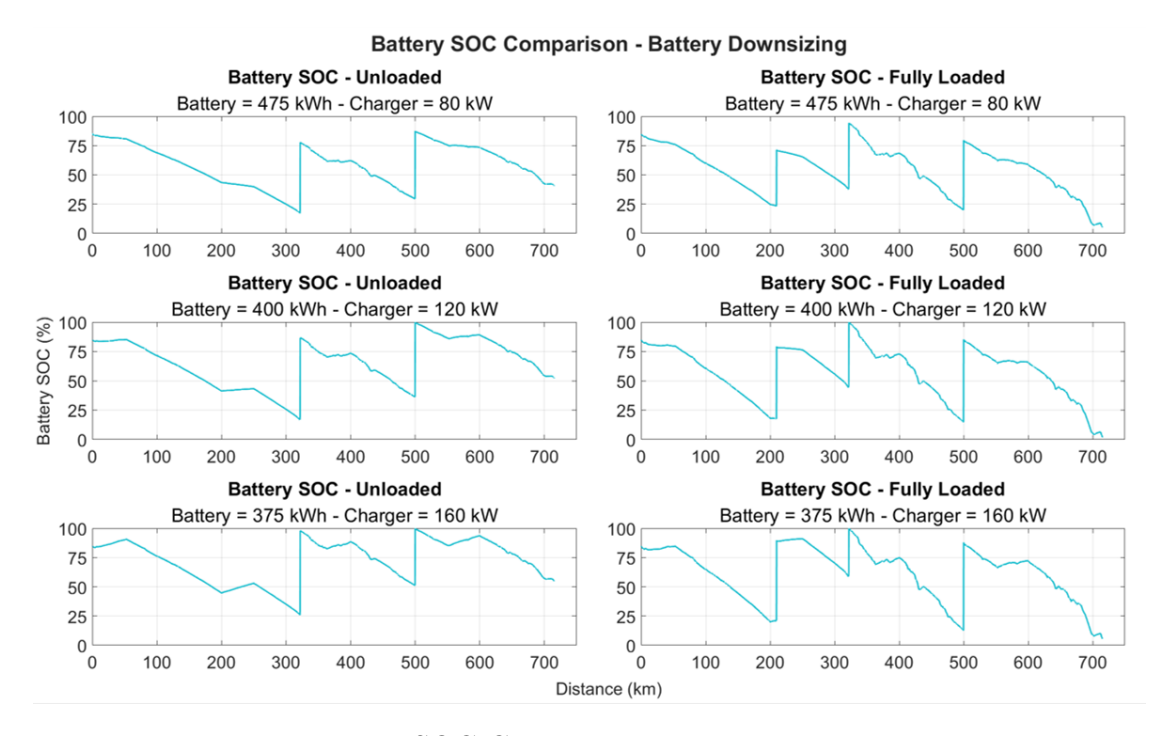


Figure 3.7: SOC Comparison - Battery Downsizing

The first notable observation concerns the effect of payload: the graphs on the left (unloaded truck) exhibit a significantly slower discharge rate compared to the right (loaded truck), where the steeper SOC decline clearly reflects the higher energy consumption required to transport the maximum payload. Consequently, the loaded configuration necessitates one additional charging stop, resulting in a longer overall mission time.

Battery downsizing leads to a sharper decrease in the residual SOC within non-electrified road segments, particularly in the 375~kWh configuration, where the SOC drops more abruptly. Nevertheless, the increased on-board charger power effectively prevents critical deep discharge events, ensuring mission completion without compromising operational feasibility.

Overall, the truck successfully completes the mission in the same total time across all configurations with equivalent loading conditions. This confirms that battery downsizing, enabled by higher on-board charging power, represents one of the most significant advantages offered by the ERS.

Table 3.4 summarises the main simulation results, including energy consumption (EC), total mission time, maximum load capability, and the utilisation ratio of each charging source. The latter is a key parameter used in the Total Cost of Ownership

TCO analysis. It was computed as the ratio between the energy supplied by a specific charging system and the total energy required to charge the truck, given by the sum of the contributions from fast charging, slow charging, and the ERS, as expressed in Equation 3.4.

$$UT_{ERS,Fast,Slow} (\%) = \frac{EC_{ERS,Fast,Slow}}{EC_{ERS} + EC_{Fast} + EC_{Slow}} \cdot 100$$
 (3.4)

Table 3.4: Simulation Results - Battery Downsizing

Technology	\mathbf{BET}		$\rm DWPT~80~kW$		$\mathrm{DWPT}\ 120\ \mathrm{kW}$		$\rm DWPT~160~kW$	
reemenegy	Unloaded	Fully Loaded	Unloaded	Fully Loaded	Unloaded	Fully Loaded	Unloaded	Fully Loaded
Battery (kWh)	700		475		400		375	
Battery Downsizing (%)	· -		32		43		46	
Maximum Payload (ton)	n) 20.1		21.4		21.8		21.9	
EC* (kWh/km)	1.166	1.577	1.161 (0.224)	$1.613\ (0.225)$	1.160 (0.336)	$1.632 \ (0.338)$	1.165 (0.448)	$1.645 \ (0.450)$
Time	$10h\ 49min$	$11h\ 26min$	10h $59min$	$11h\ 24min$	$10h\ 47min$	11h 24min	10h~47min	11h 24min
UT_{ERS} (%)	-	-	17.78	13.52	27.02	20.51	36.04	27.56
UT_{Fast} (%)	51.90	52.69	53.50	53.92	52.93	51.03	46.14	46.31
UT_{Slow} (%)	48.10	47.31	28.71	32.57	20.05	28.46	17.83	26.13

^{*} Energy between parentheses corresponds to the energy provided by the eRoad.

As expected, the configuration featuring the smallest battery and highest onboard charger power shows the greatest share of energy supplied by the ERS, consistent with the results illustrated in Figure 3.7. It is crucial to note that the EC reported for the BET represents the baseline energy demand of the mission, as the ERS contribution is zero. Therefore, the significantly lower energy consumption values observed for the DWPT are entirely attributable to the energy supplied by the eRoad.

In addition, reducing the battery size increases the maximum load capacity, demonstrating one of the most significant advantages of the ERS.

It is also important to note that the reported mission time exceeds the legal driving limit. However, this is due to the inclusion of intermediate stop durations in the total mission time, which are excluded when considering only effective driving hours.

Chapter 4

Life Cycle Assessment

This chapter presents the procedure employed to evaluate the impact assessment of the Electrified Road System, along with the results obtained.

The software used to achieve the LCA is SimaPro [42], with the database "Ecoinvent 3 - allocation at point of substitution - unit".

4.1 Goal and Scope

This study aims to evaluate the environmental impact associated with the production, construction, and maintenance of the ERS to analyse the feasibility of the system.

To this end, three utilisation scenarios were defined, representing different levels of daily adoption of the infrastructure [28]:

- Pessimistic scenario: 120 trucks charged daily;
- Average scenario: 600 trucks charged daily;
- Optimistic scenario: 1440 trucks charged daily.

Additionally, as discussed in Chapter 3, the study considers the effect of battery downsizing enabled by dynamic charging. In fact, three different on-board charger power levels were compared: $80 \ kW$, $120 \ kW$, and $160 \ kW$.

4.2 Method

4.2.1 Functional Unit (FU)

The reference electrified road section considered in this study is 1 km long and 3.5 m wide, corresponding to a single-lane, one-direction highway.

Since the analysis focuses on the use phase by BEHDT, the selected FU is the $kg\ CO_{2,eq}$.

4.2.2 System Boundary

The system boundaries adopted for this LCA study follow a cradle-to-grave model, as usage phase and refurbishment at the end-of-life are included. The model includes:

- raw material extraction and production of both the asphalt and the DWPT charging infrastructure;
- construction of the eRoad;
- asphalt maintenance and reconstruction activities throughout its lifetime.

The geographical scope is limited to Europe, in particular Italy, while the temporal scope is set to 20 years, corresponding to the expected operational lifetime of the eRoad.

4.3 LCI

This fundamental phase involves the collection of data required for modelling the ERS infrastructure. The two main components considered are the asphalt pavement, which includes the construction and maintenance phases, and the WPT system embedded within it.

4.3.1 Asphalt

The asphalt composition adopted for motorway applications was taken from the study conducted by Marmiroli et al. (2019) and is schematized in Figure 4.1.

As shown, three main layers are required for the construction of the road:

- Wearing layer, also called surface course: the uppermost layer, directly in contact with vehicle tyres. It provides abrasion resistance, weather protection, and adequate drainage, while also protecting the layers underneath it;
- Binder layer, also called intermediate course: this layer plays a crucial structural role, distributing traffic loads and contributing to the overall strength of the pavement. In the case under study, the WPT system is embedded within this layer;

• Base layer: the foundation of the road structure. It supports the upper layers, providing a stable platform for construction, and it minimises settlement under dynamic traffic loads.

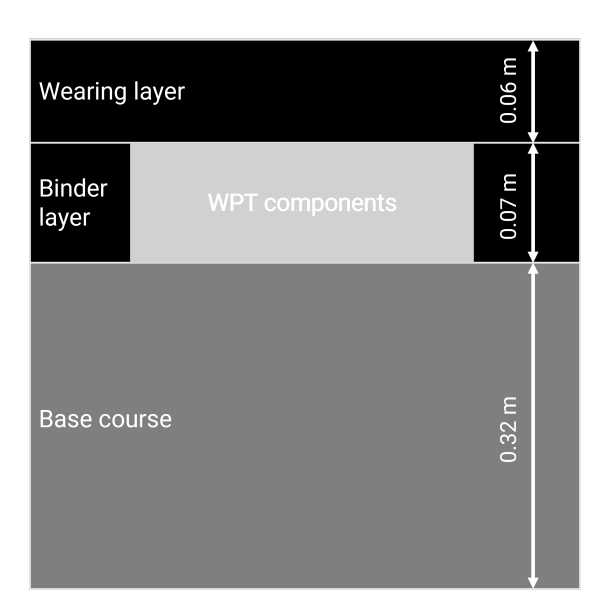


Figure 4.1: Asphalt layers

Given the thickness and the road dimensions, the volume of each layer was computed by the simple equation:

$$V_{layer} (m^3) = l \cdot b \cdot t \tag{4.1}$$

Where l and b represent the road length and width, respectively, while t is the thickness of the layer. Table 4.1 summarises the geometrical properties and topologies adopted for each layer.

Table 4.1: Asphalt Layer Composition

Layer	Thickness (m)	Volume (m^3)	Type	Regulation
Wear	0.06	210	SMA 11	UNI EN 13108-1
Binder	0.07	245	AC 20	UNI EN 13108-1
Base	0.32	1120	AC 32	UNI EN 13108-1

The *UNI EN 13108-1* [43] standard defines the specifications for Hot-Mix Asphalt (HMA) production, including the volumetric composition of its constituents

for each pavement layer, reported in Table 4.2.

Crushed Gravel Bitumen Limestone Additives Air Layer (% vol.) (% vol.) (% vol.) (% vol.) (% vol.) 7 7 2 Wear 4 80 Binder 6 8 4 81 1 Base 84 5 7 4

Table 4.2: Volumetric Composition for Each Pavement Layer

Crushed gravel is the main component of asphalt layers, providing the structural skeleton of the pavement. In the wearing layer, it also ensures surface friction and skid resistance.

Bitumen serves as the binder, providing cohesion among the aggregates and flexibility under thermal and mechanical stresses.

Limestone acts as a mineral filler, occupying voids between aggregates and improving the adhesion between bitumen and gravel, enhancing the stability of the asphalt mix.

Additives, typically polymers such as Styrene-Butadiene-Styrene (SBS), are added in small quantities to improve elasticity and thermal cracking resistance.

Once the volumetric compositions were established, the mass of each layer was calculated using the density of each material, reported in Table 4.3. The reference density values are derived from European standards: EN~1097-6~[44] for crushed gravel, EN~12591~[45] for bitumen, and EN~12620~[46] for limestone. For the additives, an average density value was assumed.

Table 4.3: Material Density

Density	Crashed Gravel	Bitumen	Limestone	Additives
$\rho \ (kg/m^3)$	2650	1030	2750	1000

The total mass of each layer was then evaluated as:

$$m (kg) = \rho (kg/m^3) \cdot \%vol. \cdot V_{layer} (m^3)$$
(4.2)

Figure 4.2 provides a graphical representation of the total mass distribution across the layers and their corresponding material composition.

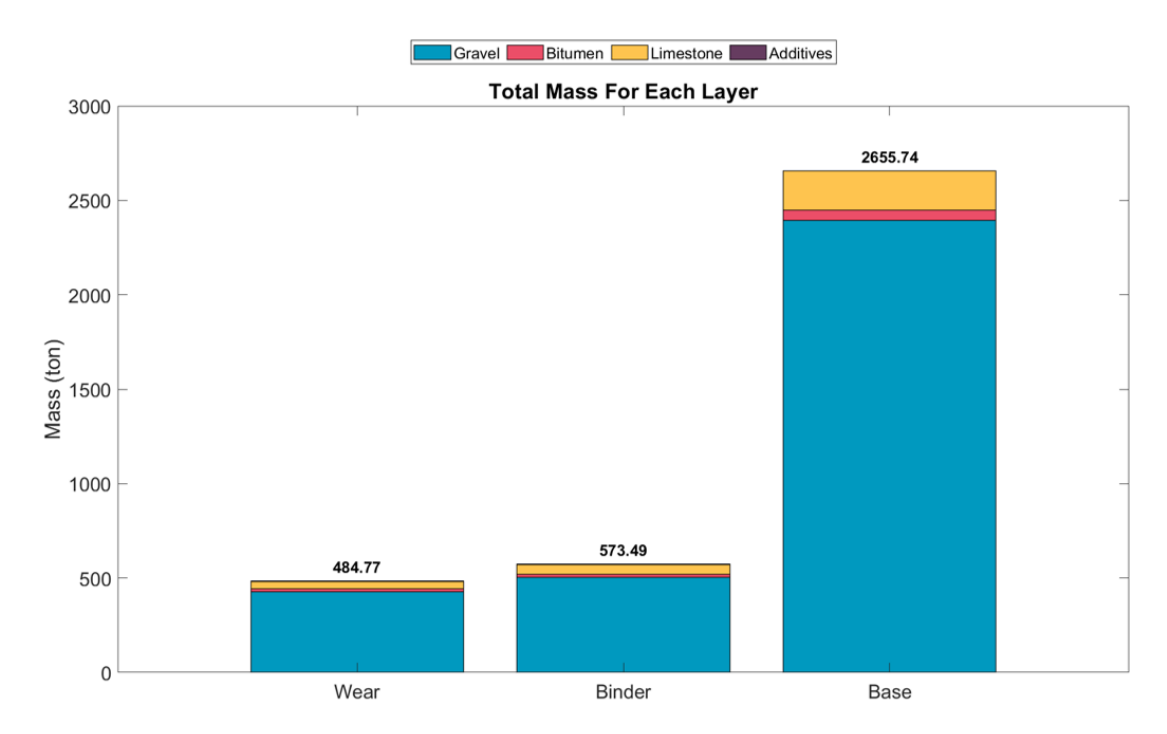


Figure 4.2: Total Mass for Each Layer

The subsequent step was the LCI implementation of the model on the SimaPro software, including the asphalt material, construction, and maintenance phases, together with the components of the WPT system.

Materials

The materials described in Section 4.3.1, used for the creation of the asphalt, are summarised in Table 4.4

Table 4.4: Asphalt Material in SimaPro

Material	Source Name in SimaPro	Layer	Quantity	Unit
Gravel	Gravel, crushed $\{RoW\}$ market for gravel, crushed APOS, U	Wear Binder Base	427392.00 504856.80 2393395.20	kg/km kg/km kg/km
Bitumen	Bitumen adhesive compound, hot $\{GLO\}\ /\ market\ for\ /\ APOS,\ U$	Wear Binder Base	14535.36 14535.36 55372.80	kg/km kg/km kg/km

Continued on next page

Material	Source Name in SimaPro	Layer	Quantity	Unit
Limestone	Cement, limestone 6–10% {RoW} market for cement, limestone 6–10% APOS, U	Wear Binder Base	38808.00 51744.00 206976.00	kg/km kg/km kg/km
Additives	Polystyrene, expandable $\{GLO\}$ / market for / APOS, U	Wear Binder Base	4032.00 2352.00 0	kg/km kg/km kg/km

Construction

The construction of an electrified road can be implemented using four main methods [47]:

- Trench-based construction: In this method, a trench is cut along the existing asphalt pavement, and the conductive unit (CU) is embedded and covered with concrete. The main advantages include a relatively low initial cost and rapid installation. Additionally, this approach enables the use of low-temperature asphalt and non-ferrous aggregates. However, it is prone to thermal cracking, which can lead to high maintenance costs;
- Micro-trench-based construction: This alternative utilises narrower slots for inserting the CU compared to the standard the trench-based. The advantages are similar to the previous one, but it also offers reduced maintenance requirements. Nonetheless, WPT coils in this configuration are more susceptible to damage caused by road traffic;
- Full-lane-width construction, in-situ build: In this configuration, the coils are embedded within a concrete structure that also protects during the paving process. This method offers low maintenance costs, improved quality, and requires only a single longitudinal joint at the lane interface. The main drawbacks are the longer construction time and potential maintenance issues related to the transversal joints;
- Full-lane-width construction, precast or prefabricated: This variant is similar to the in-situ method but employs prefabricated modules containing the coils. While it enables faster installation, the prefabricated elements may be subject to movement under heavy traffic loads.

Among these options, the most suitable approach for highway ERS application is the **Full-lane-width in-situ** method, as it ensures long-term durability and performance.

The construction process considered in this study requires the removal of both the wearing and binder layers. Therefore, the base course was not included in the *SimaPro* implementation. The construction steps are listed below [48]:

- 1. Removal of the existing wearing and binder layers using milling machines;
- 2. Debris removal using a sweeping machine;
- 3. Installation of the CU and connection to the road side;
- 4. Overlay with asphalt using a paver machine, followed by compaction with a roller;
- 5. Application of a bituminous emulsion between the two layers using an emulsion sprayer;
- 6. Installation of auxiliary equipment.

All the machinery used during construction was powered by diesel engines. Consequently, the associated emissions were modelled in SimaPro using the dataset "Diesel, low-sulfur $\{RER\}/$ market group for / APOS, U". The corresponding fuel consumption values, summarised in Table 4.5, were derived from the calculations by Marmiroli et al. [48].

Table 4.5: Machinery Fuel Consumption for Construction

Machinery	Fuel Consumption
	(kg/km)
Milling Machine	111.33
Sweeping Machine	5.01
Paver	69 (Wear layer) 29.4 (Binder layer)
Roller	786 (Wear layer) 161 (Binder layer)
Emulsion Sprayer	0.346

Maintenance

The maintenance phase is essential to ensure the proper functionality and longevity of the eRoad. As indicated by Marmiroli et al. [48], this operation should be carried out every 25 months along the service life of the ERS. Consequently, over a 20-year lifespan, maintenance activities are expected to occur ten times. Among these, one

involves the rehabilitation of both the wear and binder layers (refurbishment), one corresponds to the end-of-life intervention and therefore is not considered in the analysis, and the remaining eight consist of the rehabilitation of the wear layer only.

The main difference between the maintenance of an electrified road and a conventional one lies in the presence of the CU within the binder layer, which remains embedded in the pavement during all operations. For this reason, two types of milling machines are employed, depending on the lane area:

- Standard milling machines for lateral areas, where no CU is present;
- Fine milling machines for the central area, directly above the WPT components.

After the milling operation, a bituminous bonding layer is applied, followed by the construction of a new asphalt layer.

The fuel consumption associated with machinery used for the rehabilitation of the wear layer only, as estimated by Marmiroli et al. [48], is reported in Table 4.6.

Table 4.6: Machinery Fuel Consumption for Wear Layer Rehabilitation

Machinery	Fuel Consumption		
True IIII e I	(kg/km)		
Milling Machine	55.66		
Fine Milling Machine	20.04		
Paver	69		
Roller	786		
Emulsion Sprayer	0.346		

In the case of both wear and binder layer rehabilitation, the same machinery and construction steps are employed as in the wear layer maintenance phase. Table 4.7 summarises the corresponding fuel consumption values.

Table 4.7: Machinery Fuel Consumption for Asphalt Refurbishment

Machinery	Fuel Consumption
ivideimiery	(kg/km)
Milling Machine	132.2
Fine Milling Machine	27.83
Paver	69 (Wear layer) 29.4 (Binder layer)
Roller	786 (Wear layer) 161 (Binder layer)
Emulsion Sprayer	0.346

Transport

In accordance with Marmiroli et al. [48], the transport of machinery and asphalt materials was modelled in SimaPro using the "Transport, freight, lorry 16-32 metric ton, EURO 6 {GLO} / market for Alloc Rec, U" dataset.

The transportation distance of $50 \ km$ was assumed for both asphalt materials and construction machinery.

Table 4.8 summarises the transport impacts associated with asphalt construction, maintenance, and refurbishment.

Table 4.8: Asphalt Construction, Maintenance and Refurbishment Transport

Phase	Transport Impact		
	$(ton \cdot km)$		
Asphalt Construction	52912.8		
Asphalt Maintenance	193906.9		
Asphalt Refurbishment	52912.8		

The impacts related to asphalt construction and refurbishment were calculated by multiplying the total mass of the wear and the binder layers by the transportation distance.

Similarly, the impacts associated with asphalt maintenance were obtained by multiplying the mass of the wear layer by the transportation distance and by the number of maintenance interventions throughout the ERS lifetime.

4.3.2 DWPT

The LCI continues with the implementation of the DWPT components in *SimaPro*. The study considers both the off-board and on-board chargers.

Off-Board Charger

The infrastructure layout, shown in Figure 4.3, was developed based on the configuration proposed by Jones et al. [49].

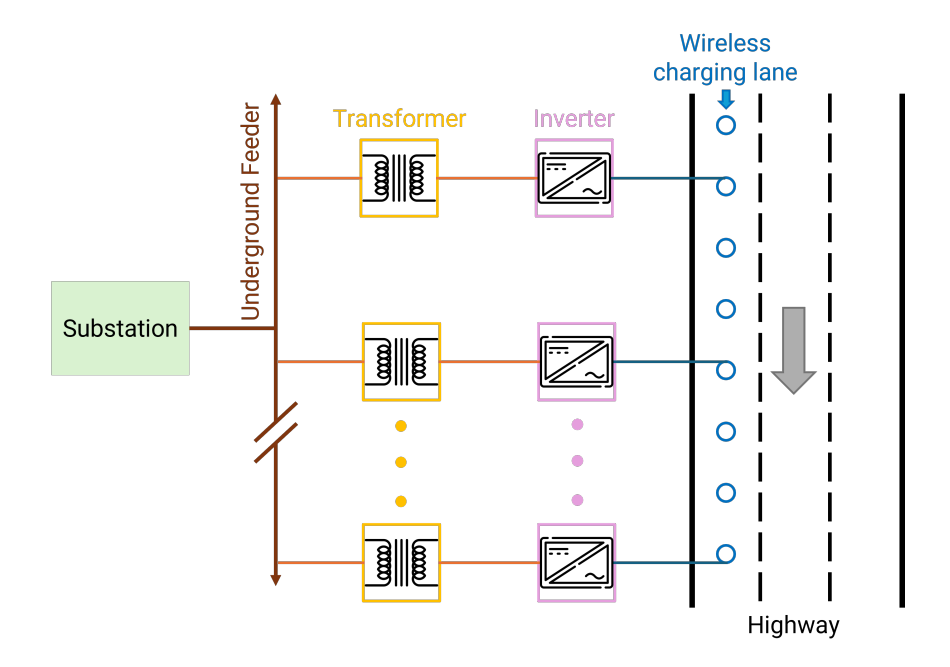


Figure 4.3: Dynamic Wireless Power Transfer Infrastructure Layout

To estimate the quantities of inverters, transformers, and coil plates required to support the maximum power deliverable by 1 km of eRoad, equivalent to $1.5 \ MW$ according to Olson et al. [50], a detailed research was performed.

The number of coil plates was determined using the 6~kW coil plate specifications provided by Bi et al. [51], resulting in a total of 250 units per kilometre. Since one inverter is required for every 50 coils [48], the number of inverters, and consequently of transformers, was limited to five. The remaining components were derived from the supplementary material provided by Bi et al. [52].

Table 4.9 summarises the data implemented in SimaPro.

Table 4.9: DWPT Infrastructure Components

Component	Source Name in SimaPro	Quantity per km	Unit
Underground Feeder	Transmission network, electricity, high voltage $\{RoW\}/$ construction $ APOS, U $	0.6214	km
Connecting Wires	Cable, three-conductor cable $\{GLO\}/$ market for $/$ APOS, U	894.97	m
Inverters	Inverter, $500kW$ {GLO}/ market for / APOS, U	5	pieces
Transformers	Transformer, low voltage use $\{GLO\}/$ market for $/$ APOS, U	1700	kg
Coil Plates	See Table 4.10	250	pieces

Each coil plate was modelled in SimaPro following the specifications provided by [51]. The details are presented in Table 4.10

Table 4.10: Coil Plate Components

Component	Source Name in SimaPro	Quantity per km	Unit
Pure Copper Wire	Copper, cathode $\{GLO\}/$ market for $ APOS,\ U$	2.4447	kg
Enamel	Alkyd paint, white, without solvent, in 60% solution state {RER}/ market for alkyd paint, white, without solvent, in 60% solution state / APOS, U	0.0247	kg

Continued on next page

Component	nent Source Name in SimaPro		Unit
Polyester	Polyethylene terephthalate, granulate, amorphous {Europe without Switzerland}/ polyethylene terephthalate, granulate, amorphous, recycled to generic market for amorphous PET granulate / APOS, U	0.0545	kg
Capacitors (film)	Capacitor, film type, for through-hole mounting {GLO}/ market for APOS, U	0.1699	kg
Printed Circuit Board	Printed wiring board, surface mounted, unspecified, Pb free {GLO}/ market for / APOS, U	0.080	kg
Ferrite Bars	Ferrite {GLO}/ market for / APOS, U	4.680	kg

On-Board Charger

To account for the impact of the receiving coil on the truck, which is fundamental for the dynamic charging of the vehicle, the same 6 kW coil plate described in Table 4.10 was used, in the amount required for each charger configuration.

Transport

In accordance with Marmiroli et al. [48], the transport of DWPT components was modelled in SimaPro using the "Transport, freight, lorry 3.5-7.5 metric ton, $EURO\ 6\ \{GLO\}\ /\ market\ for\ Alloc\ Rec,\ U"$ dataset to estimate the associated environmental impact.

The transport distance and component mass were assumed to be 100 km and 10 tons, respectively. This results in a total transport activity of 1000 $ton \cdot km$ for the DWPT components.

4.3.3 Energy Delivered

Another relevant aspect concerns the assessment of the climate impact during the usage phase. This evaluation is presented mainly as an illustrative example of how

the methodology can be applied and is not directly related to the specific impact of the ERS.

In this context, the climate impact associated with the energy supplied to the truck was analysed. To investigate the influence of different electricity sources, four scenarios were considered:

- 1. The Italian electricity mix: Electricity, low voltage {IT}/ market for / APOS, U;
- 2. Hydroelectric power: Electricity, high voltage {IT}/ electricity production, hydro, reservoir, alpine region / APOS, U;
- 3. Solar power: Electricity, low voltage {IT}/ electricity production, photovoltaic, 3kWp slanted-roof installation, multi-Si, panel, mounted / APOS, U;
- 4. Wind power: Electricity, high voltage {IT}/ electricity production, wind, >3MW turbine, onshore / APOS, U.

The climate impact was assessed for all three vehicle utilisation scenarios over the entire ERS lifetime. For each case, the energy consumption under payload conditions, reported in Table 3.4, was multiplied by the number of trucks per day and the number of days in 20 years, which, considering five leap years, corresponds to a total of 7305 days. The results are reported in Table 4.11.

Energy Delivered (GWh/km) Charger Power 80 kW 120 kW 160 kW Optimistic 14.6 13.6 12.6 Scenario Average 6.1 5.7 5.2 Pessimistic 1.2 1.1 1.0

Table 4.11: Energy Delivered

4.4 Impact Assessment and Interpretation

This phase of the life cycle assessment presents the results obtained using the European "EF 3.0 Method (adapted)" to evaluate the climate impact of the ERS.

4.4.1 Asphalt

Materials

Figure 4.4 shows the climate impact of the materials composing the wear and binder layers of the asphalt listed in Table 4.4.

The climate change impact is expressed in the chosen FU, $kgCO_{2eq}$, and is broken down by the individual materials composing the asphalt layers.

The impacts of the binder and wear layers are of the same order of magnitude, with the binder layers contributing slightly more due to the larger quantity of material required.

Among the materials composing both layers, limestone has the highest impact. Although its volumetric percentage is relatively small, its extraction and production processes are highly energy-intensive and generate significant amounts of greenhouse gas emissions.

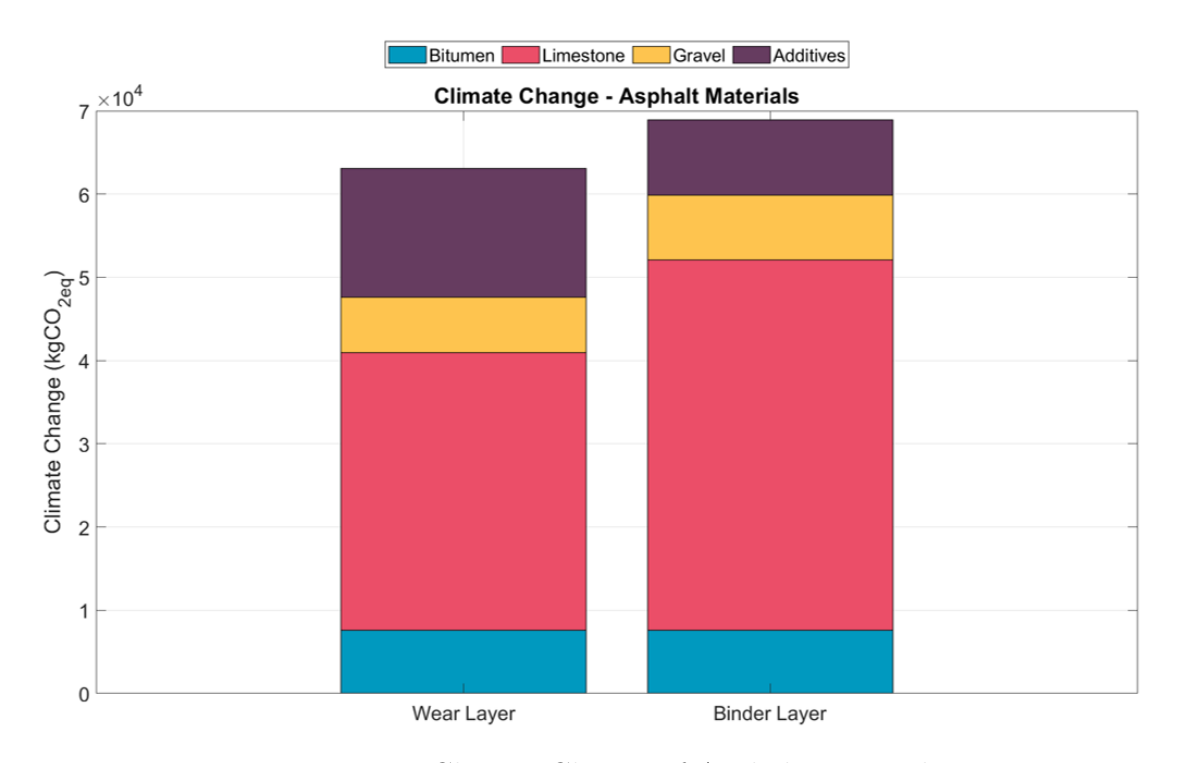


Figure 4.4: Climate Change of Asphalt Materials

Construction, Maintenance and Transport

Figure 4.5 illustrates the total impact generated by the asphalt materials, the construction phase, wear layer maintenance, and refurbishment over the 20-year

lifetime of the ERS.

The figure distinguishes the impacts associated with the materials and machinery used during asphalt construction and maintenance.

It can be observed that the construction phase has the lowest climate impact, as it only accounts for the emissions produced by the machinery used, with the roller machine being the most significant contributor.

The asphalt production and refurbishment phases are quite similar, the main difference is that refurbishment also includes the construction phase, whereas asphalt production accounts only for the materials and their transport. This reflects that refurbishment essentially involves reconstructing the asphalt at the end of the ERS lifetime.

Finally, the most impactful activity is the wear layer maintenance, corresponding to the cumulative effect of the eight maintenance phases over the ERS lifetime. As expected, the wear layer itself contributes the most to this impact.

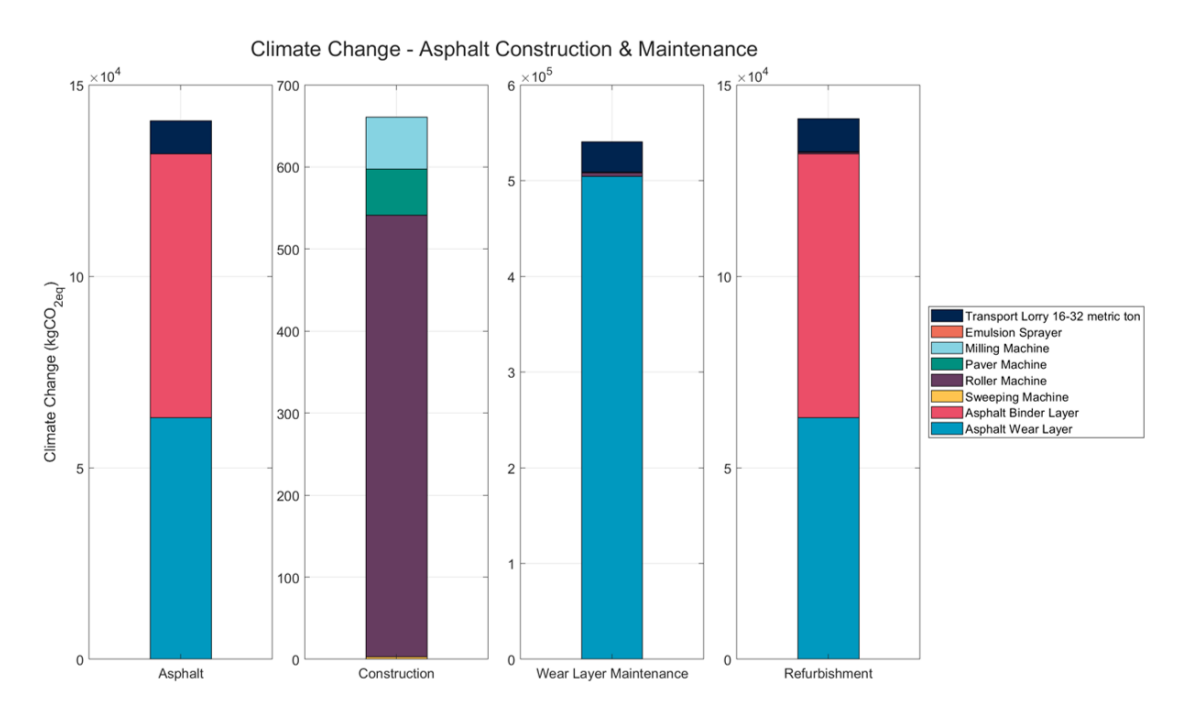


Figure 4.5: Climate Change of Asphalt Construction and Maintenance

Summary Table

The following table summarises the results obtained from the impact assessment of the asphalt.

Table 4.12: Asphalt Summary Table

Category	Climate Change		
	$(kgCO_{2eq})$		
Wear Layer	63049		
Binder Layer	68928		
Asphalt	131978		
Asphalt Construction	661		
Asphalt Maintenance	508543		
Asphalt Refurbishment	132572		
Total Asphalt Impact	905731		

4.4.2 DWPT

Off-Board Charger

Figure 4.6 shows the climate impact of the materials required to produce the off-board charger for 1 km of eRoad. The most impactful components are the inverter and the underground feeder, while the smallest contribution, aside from transportation, is given by concrete.

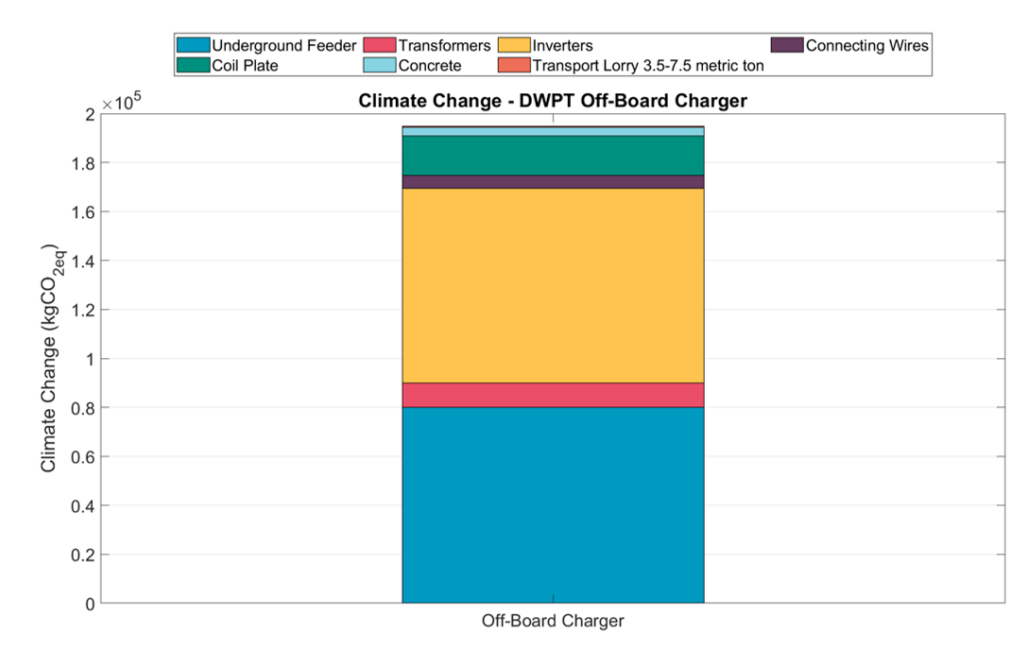


Figure 4.6: Climate Change of Off-Board Charger

Figure 4.7 provides a detailed description of the coil plate used in the off-board charger. The main contributors are the printed wiring board and the copper.

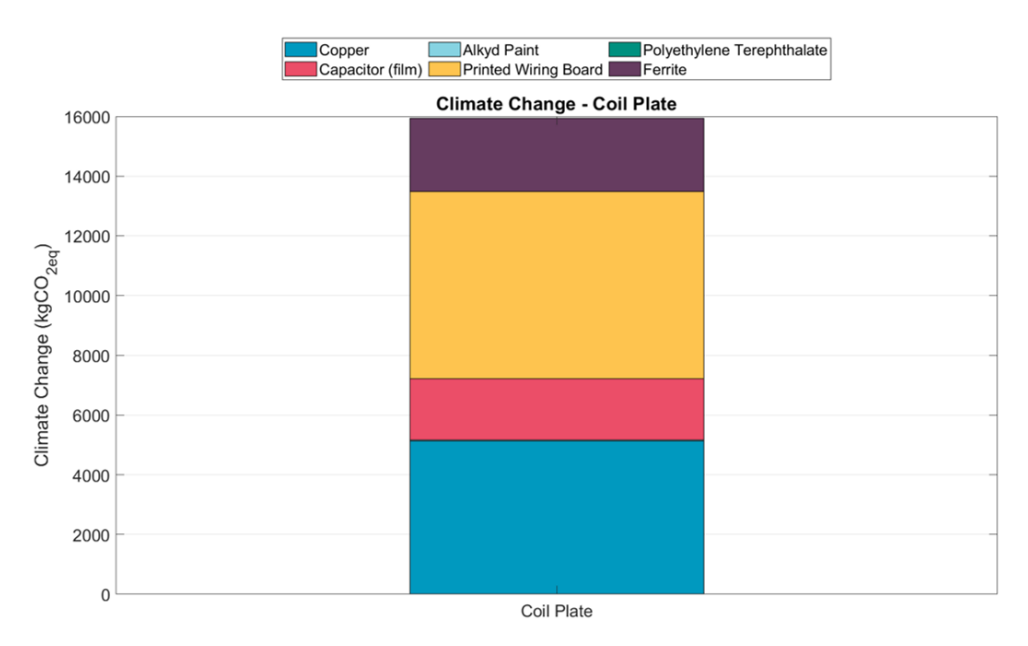


Figure 4.7: Climate Change of Coil plate

On-Board Chargers

Figure 4.8 compares the climate impact of the three on-board charger power configurations.

As described in Section 4.3.2, the on-board chargers were modelled as coil plates in quantities required to achieve each power configuration. For this reason, the distribution of impacts among the charger components is the same, with contributions increasing proportionally with charger power.

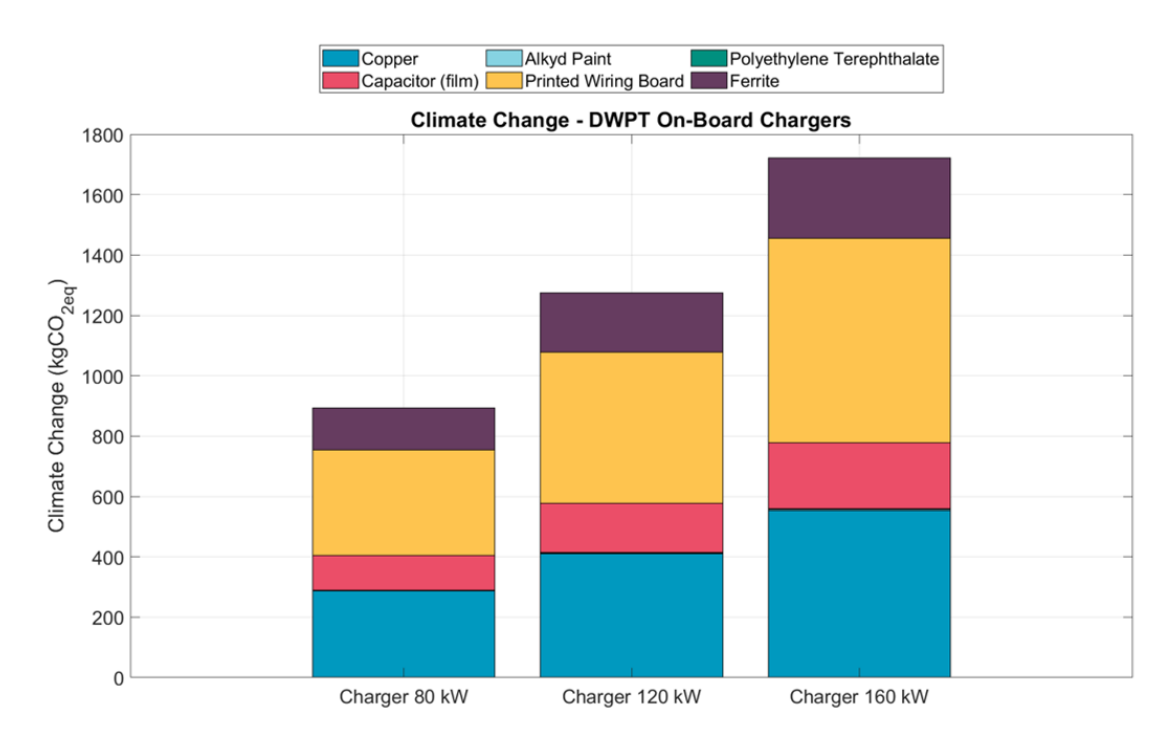


Figure 4.8: Climate Change of On-Board Chargers

Summary Table

Table 4.13 summarises the climate impact results of the DWPT components.

Table 4.13: DWPT Summary Table

Category	Climate Change	
catogory	$(kgCO_{2eq})$	
Off-Board Charger	194342	
Coil Plate	15943	
On-Board Charger 80 kW	893	
On-Board Charger 120 kW	1275	
On-Board Charger 160 kW	1722	

4.4.3 1 km of ERS

Figure 4.9 illustrates the contribution of each component to the overall climate impact associated with the implementation of 1 km of ERS over its lifetime, considering 475 kWh battery, 80 kW on-board charger and the average utilisation ratio scenario.

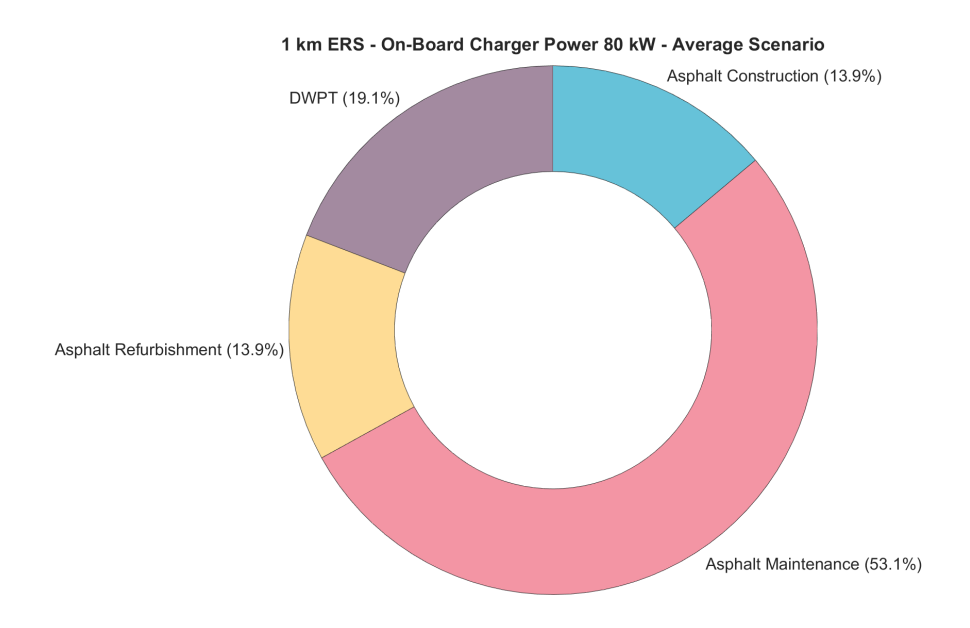


Figure 4.9: Breakdown of Climate Impact for 1 km of ERS

It is possible to notice that the major contribution is given by the eight maintenance phases during the service life of the ERS, as already highlighted in Figure 4.5.

4.4.4 Energy Delivered

This section compares the climate impacts associated with different electricity sources used for energy delivery.

It is important to highlight that this analysis focuses exclusively on the usage phase and is therefore presented as a general illustrative case. For this reason, only the first configuration, corresponding to the $475\ kWh$ battery and $80\ kW$ on-board charger under full-load conditions, is presented.

As shown in Figure 4.10, the electricity mix results in the highest climate impact, as expected. Instead, among renewable sources, hydroelectric power is the least impactful, followed by wind and solar power.

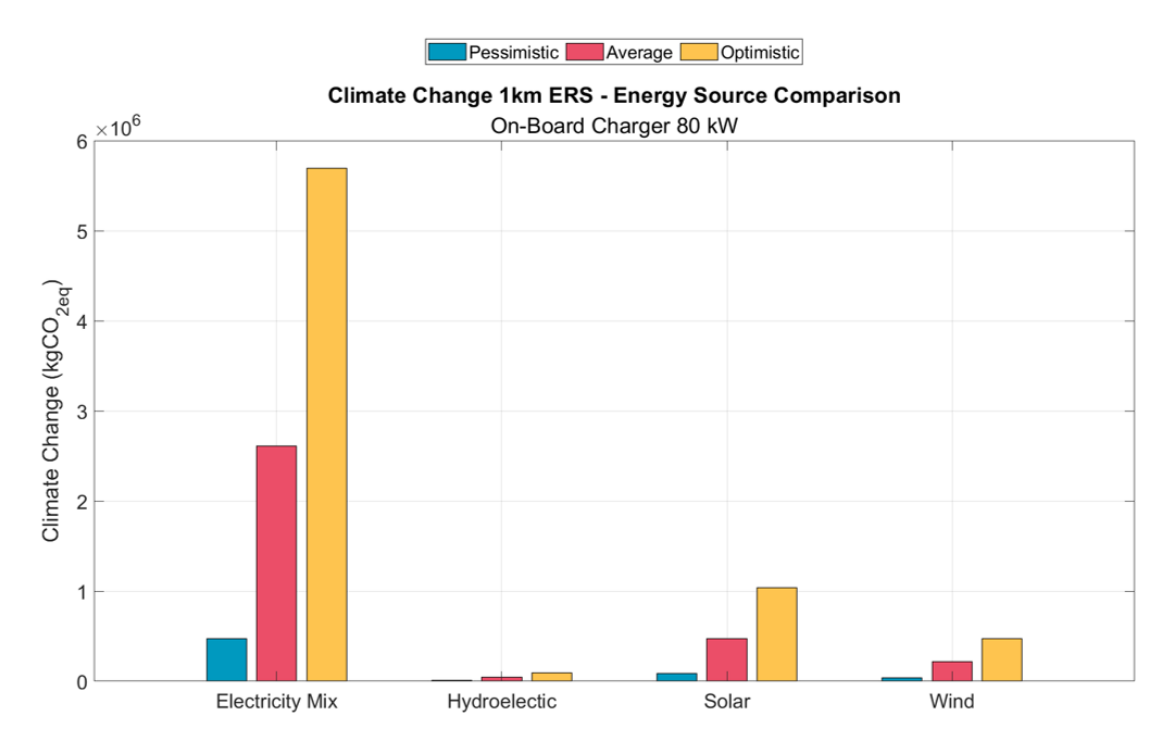


Figure 4.10: Climate Change and Energy Source Comparison

Summary Table

Table 4.14 summarises the climate impacts associated with the energy delivered from four different energy sources, considering all three on-board charger power levels and the three utilisation ratios.

Due to the lower energy consumption of the 160 kW on-board charger and the 375 kWh battery capacity, the overall climate impact associated with energy delivered by the ERS decreases accordingly.

Table 4.14: Energy Delivered Summary Table

On-Board Charger Power (kW)	Utilization Case	Climate Change $(kgCO_{2eq})$			
on Board Charger 1 over (iiii)		Electricity Mix	Hydroelectric	Solar	Wind
	Pessimistic	474223	7765	86386	39261
80	Average	2608226	42707	475123	215935
	Optimistic	5690675	93179	1036633	47113
	Pessimistic	442107	7239	80536	36602
120	Average	2431588	39815	442946	201311
	Optimistic	5305283	86869	966428	439225
	Pessimistic	408283	6685	74374	33802
160	Average	2245555	36769	409058	185910
	Optimistic	4899392	80222	892490	405621

4.4.5 Comparison Between BET and DWPT

This section compares the life-cycle climate impact of a conventional BET with that of a truck equipped with DWPT. In this case the cradle-to-gate approach was employed.

According to Di Vittorio et al. [53], the climate impact associated with the production of a Li-ion battery is approximately 119.7 $kgCO_{2eq}/kWh$.

Based on this reference value, the total climate impact of the conventional BET was calculated by multiplying the specific battery impact by its capacity. In the case of the BET equipped with DWPT, the climate impact of the on-board charger components was additionally considered.

Figure 4.11 shows the percentage variation in total climate impact across the three analysed scenarios. It is evident that the overall reduction is primarily driven by the smallest battery capacity, while the additional impact of the on-board charger is negligible in comparison.

Overall, the results demonstrate that battery downsizing significantly decreases the life-cycle climate impact, achieving approximately 31%, 41%, and 44% reductions in the first, second, and third scenarios, respectively.

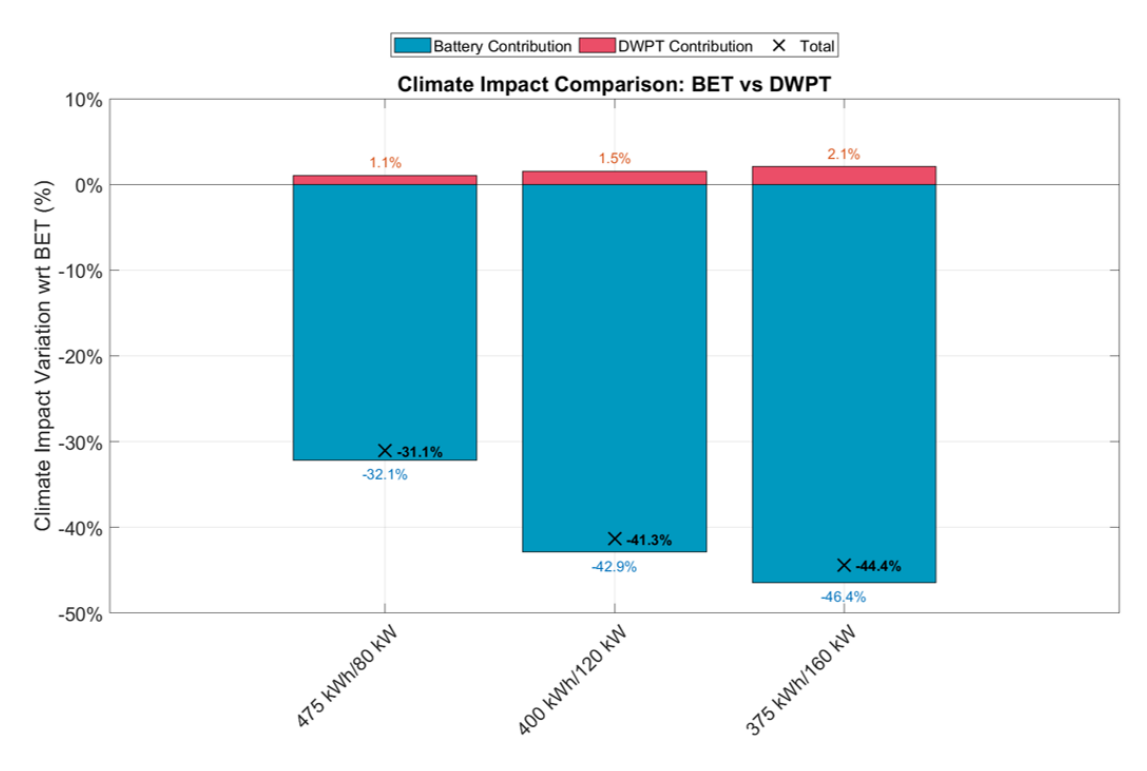


Figure 4.11: Comparison of Climate Impact Breakdown between BET and DWPT

Chapter 5

Total Cost of Ownership

This chapter presents and discusses the results obtained from the TCO analysis. At the beginning, the most relevant input data are highlighted to provide a clear overview of the assumptions adopted. The analysis was carried out using the programming language *Python*, implementing the equations introduced in Section 2.4. The simulation results under maximum payload, summarised in Table 3.4, were used as input data.

5.1 Scenarios and Data

To provide a comprehensive understanding of the cost associated with the deployment of the ERS, as done for the life cycle assessment, three utilisation scenarios (optimistic, average and pessimistic) were developed. These scenarios correspond to different levels of ERS usage, leading to different cost distribution among the changing technologies. For each combination of on-board charger power and battery size, the utilisation ratio (UT) was applied in Equations 2.7 and 2.8.

Table 5.1 summarises the UT adopted for each scenario and charging technology: slow charging at $100 \ kW$ at the end of the mission, fast charging at $350 \ kW$ during the scheduled stops, and eRoad charging at 80, 120 and $160 \ kW$.

Table 5.1: Utilisation Ratio

Utilisation Ratio (%)					
Recharging Technology		Slow Charging	Fast Charging	eRoad	
	Optimistic	33	12	12	
Scenario	Average	20	5	5	
	Pessimistic	10	1	1	

To evaluate the Net Present Value (NPV), in Equation 2.3, the discount rate r was set to 10%, following the reference study by Costantino et al. [28]. Consistently, the Internal Rate of Return (IRR), introduced in Equation 2.4, was differentiated according to the infrastructure type: a value of 4% was assumed for slow chargers, while a higher rate of 10% was applied for both fast chargers and the eRoad.

Regarding capital expenditures, the reference scenario was based on the estimates provided in the literature. In particular, Hutchinson et al. [54] reported the cost of constructing 1 km of ERS to approximately \in 5 million, adopted as baseline input for the year 2022. Similarly, the purchase cost of DWPT components was set at 185 \in /kW, as reported by Gill et al. [55].

To extend the analysis beyond current conditions and provide a more comprehensive perspective, future scenarios for the years 2030 and 2050 were also considered. In these projections, reductions in both electricity prices and subsystems purchase costs were assumed, reflecting potential benefits from economies of scale, technological innovation, and market standardisation. Since official forecasts for future capital expenditures of the ERS are not yet available, the analysis relies on estimated cost reductions: specifically, a 15% decrease by 2030 and a 40% decrease by 2050. These assumptions enable the evaluation of long-term trends and the potential impact of cost reductions on the overall system feasibility.

5.2 TCO Results

In this section, the results of the TCO analysis are presented in terms of \in /ton·km, considering a lifetime of 700000 km for the truck and the maximum transportable payload for each configuration.

5.2.1 Total Cost of Ownership

Figure 5.1 illustrates the results obtained for the different utilisation scenarios under maximum payload conditions. The analysis reveals that the largest cost component is represented by the energy carrier, reflecting the electricity required to power the vehicle. This value is directly influenced by the energy consumption evaluated in the simulation and shows a progressive decrease in the future scenarios. Indeed, a 37% reduction in electricity prices in Italy is expected by 2030, with a further 41% reduction by 2050 [28].

The results also indicate that the DWPT technology becomes economically feasible under the average scenario, with this trend becoming even more pronounced in the optimistic one. Furthermore, these findings are enhanced by the advantage of a higher maximum payload capacity enabled by battery downsizing.

Focusing on the on-board charger configurations, the 160~kW case shows the highest total cost in the pessimistic scenario. This is primarily linked to the higher utilisation ratio of the DWPT system, as also reported in Table 3.4. Conversely, the vehicle purchase cost tends to decrease as the on-board charger power increases. This trend can be explained by the reduction in battery size enabled by the use of the ERS, which lowers both the initial investment and the associated operational costs.

Other cost components, such as taxes, driver cost and maintenance, remain constant across all scenarios and technologies, and therefore do not significantly affect the comparison.

Finally, the residual value is strongly influenced by the battery capacity, as also highlighted by Equation 2.9. A smaller battery results in a lower initial purchase cost but also leads to a reduced residual value at the end of the vehicle's lifetime.

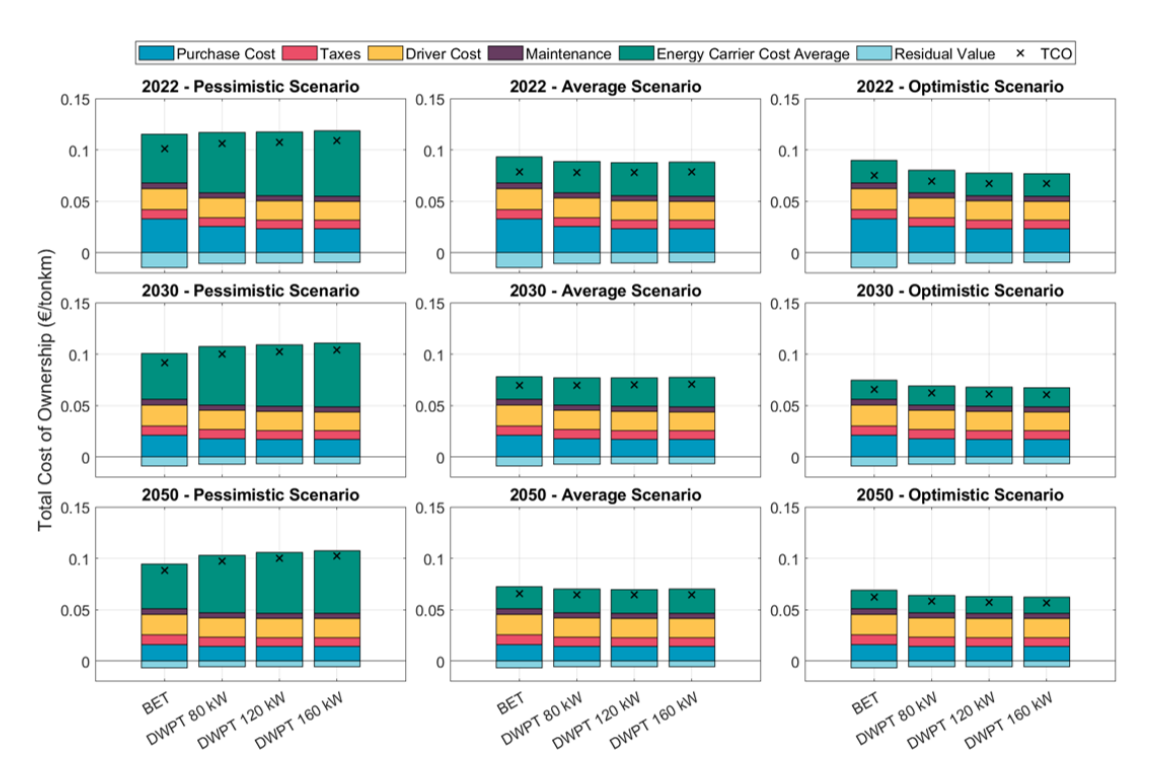


Figure 5.1: TCO for Different Technologies, Utilisation Ratio and Future Scenarios

Table 5.2 summarises the average TCO values for each technology configuration and scenario.

Table 5.2: Total Cost of Ownership

TCO $(\in/ton \cdot km)$					
Year	Scenario	BET	Charger 80 kW	Charger 120 kW	Charger 160 kW
2022	Pessimistic	0.101	0.106	0.108	0.109
	Average	0.079	0.078	0.078	0.079
	Optimistic	0.075	0.069	0.068	0.067
2030	Pessimistic	0.092	0.100	0.102	0.104
	Average	0.069	0.070	0.070	0.071
	Optimistic	0.066	0.062	0.061	0.061
2050	Pessimistic	0.088	0.097	0.100	0.102
	Average	0.066	0.065	0.064	0.064
	Optimistic	0.062	0.059	0.057	0.057

The results highlight that the pessimistic scenario represents the worst case, where TCO parity is never achieved. On the contrary, in the average and, in a more pronounced way, in the optimistic scenario, the DWPT technology becomes economically feasible. These findings emphasise the crucial role of battery downsizing in achieving TCO parity.

5.2.2 Purchase Cost Breakdown

Figure 5.2 illustrates the contribution of each truck subsystem to the total purchase cost. For the sake of simplicity, the figure refers to the baseline scenario of 2022 and the results are expressed in $\in k$ to show the purchase cost of each subsystem.

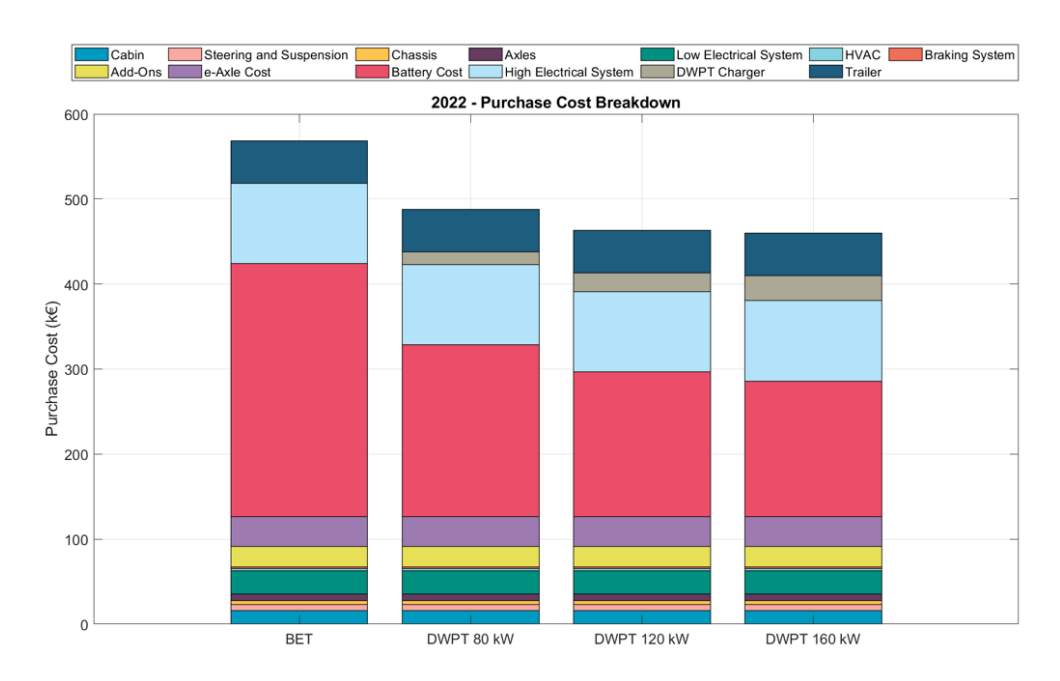


Figure 5.2: Purchase Cost Breakdown, year 2022

It is clearly visible how the adoption of DWPT technology leads to a reduction in overall purchase cost. This effect is primarily driven by the downsizing of the battery, which significantly lowers the battery-related cost component (evidenced by the red bar). As expected, the cost associated with the DWPT system increases with the on-board charger power.

All other components remain unchanged, since only the powertrain configuration was modified across the analysed cases.

5.2.3 Energy Carrier Cost Breakdown

Figure 5.3 provides a detailed breakdown of the energy carrier cost across the different charging technologies, referring also in this case to the 2022 baseline scenario.

The results are consistent with the simulation outputs reported in Table 3.4. As the on-board charger power increases, the utilisation ratio of both fast and slow charging decreases, while the share of energy supplied by the ERS grows accordingly.

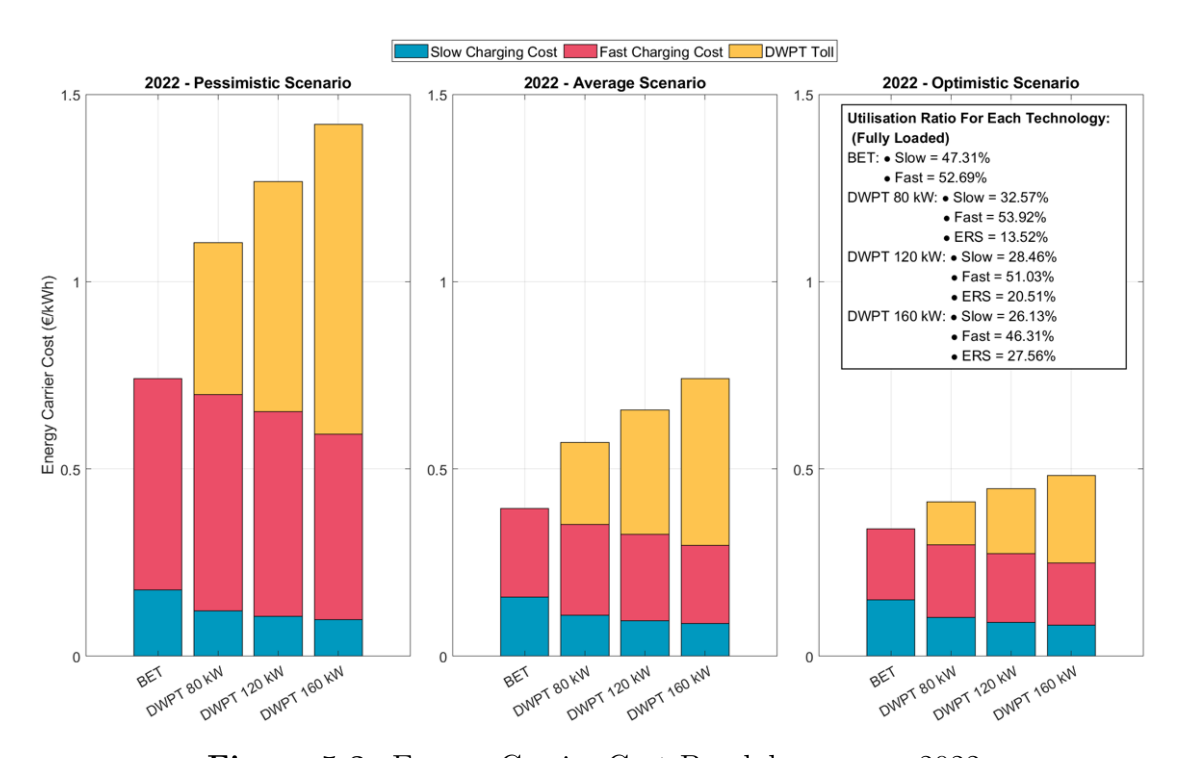


Figure 5.3: Energy Carrier Cost Breakdown, year 2022

5.2.4 BET and DWPT TCO Parity Analysis

This section investigates the influence of the three key ERS parameters on the achievement of TCO parity between the BET and the DWPT configurations in the pessimistic 2022 scenario.

In particular, the objective is to determine the values of Internal Rate of Return IRR, capital expenditure CAPEX, and utilisation ratio (UT) of the ERS that satisfy the condition:

$$TCO_{DWPT}(ECC) - TCO_{BET} = 0 (5.1)$$

Where $TCO_{DWPT}(ECC)$ is the total cost of ownership for the DWPT technology in function of the energy carrier cost.

The calculation was implemented in *Python* using the fsolve function, starting from the initial baseline parameter reported in Table 5.3.

Table 5.3: Initial Baseline Parameter

Scenario	IRR_{ERS}	$CAPEX_{ERS}$	UT_{ERS}	TCO_{BET}	Initial ERS Tariff
	(-)	(€M)	(%)	$({\in}/ton\cdot km)$	(\in /kWh)
Pessimistic	0.1	5	1	0.101	3

Since the system is defined by a single equation with three variables, the analysis was conducted by varying one parameter at a time while keeping the others constant.

This approach allows the estimation of the level of governmental incentives required to make the ERS investment economically competitive.

The results indicate that achieving TCO parity by acting only on the IRR would require a negative value, which is not realistic from an investment perspective. Conversely, for the other two parameters, Equation 5.1 can be solved, leading to the results reported in Table 5.4.

Table 5.4: TCO Parity

Variable	IRR_{ERS}	UT_{ERS}	$CAPEX_{ERS}$	New ERS Tariff	Δ Tariff
V 012 141.0 10	(-)	(-)	(€M)	(€/kWh)	(€/kWh)
$f(UT_{ERS})$	0.1	0.0338	5	2.255	0.745
$f(CAPEX_{ERS})$	0.1	0.01	1.48	2.200	0.140

Where Δ Tariff is the difference: Tariff $_{ERS}^{Initial}$ – Tariff $_{ERS}^{NEW}$. This difference was used to compute the government incentives, recalling Equation 2.8, as:

Incentives =
$$\Delta \text{Tariff} \cdot ES_y \cdot \text{Lifespan}_{ERS}$$
 (5.2)

Leading to the government incentives summarised in Table 5.5:

Table 5.5: Government Incentives

Variable	Incentives $(\in M)$			
	(€M)			
$f(UT_{ERS})$	6.62			
$f(CAPEX_{ERS})$	1.96			

The results align with the expectations: an increase in the utilisation ratio (meaning a higher number of trucks using the ERS) permits the distribution of the fixed cost over a larger amount of energy delivered. Similarly, a reduction in CAPEX decreases the initial investment to be amortised, thereby directly reducing the overall TCO and improving the economic feasibility of the system.

Chapter 6

Conclusions

The thesis aimed to investigate the techno-economic and environmental feasibility of an Electrified Road System (ERS) based on Dynamic Wireless Power Transfer (DWPT) for long-haul Battery Electric Heavy-Duty Trucks (BEHDTs).

The analysis mainly focused on assessing whether ERS could overcome the current limitations of fully electric trucks, such as limited driving range, long recharging times, and payload reduction due to battery weight.

The study, carried out along 715 km real-world route between Torrazza (Piedmont) and Colleferro (Lazio), demonstrated that integrating 200 km of electrified road segments, corresponding to around 30% of the route, allows for:

- Battery downsizing of up to 46%, while still completing the same mission profile;
- Increase in maximum load capacity by up to 1.8 tons, achieved through the reduction of battery mass. This improvement translates into lower transport cost per $ton \cdot km$;
- Reduction in truck climate impact by approximately 44% mainly due to lower raw material requirements and reduced emissions from battery manufacturing;
- Dynamic charging capability, with the ERS supplying up to 36% of total energy demand, depending on on-board charger power and payload conditions.

Nevertheless, the Life Cycle Assessment (LCA) revealed that the major contributor to the climate impact $(CO_{2,eq})$ is the road maintenance phase.

From an economic standpoint, the Total Cost of Ownership (TCO) analysis showed that the ERS can achieve cost parity or even economic advantage over BET under average and optimistic utilisation scenarios. Under pessimistic conditions, cost parity in 2022 would require government incentives of approximately 6.62M or

 $\in 1.96M$, depending on the economic parameter being adjusted.

These results confirm the technical potential of the ERS to decarbonise long-haul freight transport by effectively mitigating range limitations, lowering battery-related emissions, and improving payload efficiency, which ultimately reduces the transportation cost per unit of cargo. However, the system remains economically demanding, requiring substantial initial investment, a high utilisation rate, and policy support to enable large-scale implementation.

In conclusion, the ERS represents a technically viable yet economically demanding solution for the decarbonisation of heavy-duty road transport.

With continued technological progress, cost optimisation, and supportive public policies, ERS could become a key enabler of sustainable, large-scale electrified freight transport across Europe.

6.1 Future Works

Although the results of the study are encouraging, several refinements, validations and real-world implementations in future works could consolidate and expand the findings. The main proposed improvements are:

- Optimisation of ERS Segments Distribution: future analyses should focus on developing optimisation models to determine the most efficient length, spacing, and positioning of eRoad segments along the route. These models should consider traffic density, vehicle flow, and the availability of static charging stations;
- Optimisation of Fast Charging Stops: The optimisation model should also include the study of the most suitable locations and scheduling of fast charging stops, from both temporal and economic perspectives;
- Expansion of the Case Study: the analysis should be extended to different routes and mission profiles to assess the proposed solution under diverse environmental, operational, and logistic conditions;
- Primary Data for the Economic Model: future work should incorporate primary cost data, for truck purchase price breakdown and maintenance expenses. This would improve the accuracy of the TCO assessment;
- Impact analysis on Battery Ageing: future research should investigate the influence of ERS operation on battery degradation and lifespan;
- Real-World Test and Data Validation: the next step is to adopt data collected from the vehicle's ECU through a real-world project. This would enable the

collection of data on dynamic charging efficiency, infrastructure wear, and actual energy consumption under different operating conditions.

Bibliography

- [1] Heavy-duty vehicles. en. URL: https://climate.ec.europa.eu/eu-action/transport-decarbonisation/road-transport/heavy-duty-vehicles_en (visited on 06/12/2025) (cit. on p. 1).
- [2] Sustainable Development Goals European Commission. en. URL: https://international-partnerships.ec.europa.eu/policies/sustainable-development-goals_en (visited on 06/15/2025) (cit. on p. 1).
- [3] Regulation (EU) 2019/1242 of the European Parliament and of the Council of 20 June 2019 setting CO₂ emission performance standards for new heavy-duty vehicles and amending Regulations (EC) No 595/2009 and (EU) 2018/956 of the European Parliament and of the Council and Council Directive 96/53/EC (Text with EEA relevance). en. Legislative Body: OP_DATPRO. July 2024. URL: http://data.europa.eu/eli/reg/2019/1242/2024-07-01/eng (visited on 06/15/2025) (cit. on p. 1).
- [4] Regulation EU 2024/1610 EN EUR-Lex. en. Doc ID: 32024R1610 Doc Sector: 3 Doc Title: Regulation (EU) 2024/1610 of the European Parliament and of the Council of 14 May 2024 amending Regulation (EU) 2019/1242 as regards strengthening the CO2 emission performance standards for new heavy-duty vehicles and integrating reporting obligations, amending Regulation (EU) 2018/858 and repealing Regulation (EU) 2018/956 (Text with EEA relevance) Doc Type: R Usr_lan: en. URL: https://eur-lex.europa.eu/eli/reg/2024/1610/oj/eng (visited on 06/15/2025) (cit. on p. 1).
- [5] Martin. Communications materials. en-US. URL: https://www.un.org/sustainabledevelopment/news/communications-material/(visited on 06/15/2025) (cit. on p. 2).
- [6] Georgios Fontaras, Martin Rexeis, P. Dilara, Stefan Hausberger, and Konstantinos Anagnostopoulos. «The Development of a Simulation Tool for Monitoring Heavy-Duty Vehicle CO₂ Emissions and Fuel Consumption in Europe». In: SAE Technical Papers 6 (Sept. 2013). DOI: 10.4271/2013-24-0150 (cit. on p. 2).

- [7] Marc Sens. «Hybrid powertrains with dedicated internal combustion engines are the perfect basis for future global mobility demands». In: *Transportation Engineering* 13 (2023). ISSN: 2666-691X. DOI: https://doi.org/10.1016/j.treng.2022.100146. URL: https://www.sciencedirect.com/science/article/pii/S2666691X22000446 (cit. on p. 5).
- [8] Paul Arévalo, Marcos Tostado-Véliz, Daniel Icaza-Álvarez, and Francisco Jurado. «Chapter 12 Hydrogen-based automotive applications: a promising future». In: *Hydrogen Energy Conversion and Management*. Ed. by Mohammad Masud Kamal Khan, Abul Kalam Azad, and Amanullah Maung Than Oo. Elsevier, Jan. 1, 2024, pp. 395–428. ISBN: 978-0-443-15329-7. DOI: 10.1016/B978-0-443-15329-7.00002-8. URL: https://www.sciencedirect.com/science/article/pii/B9780443153297000028 (visited on 10/11/2025) (cit. on p. 5).
- [9] Xingyu Xue et al. «Life Cycle Economic and Environmental Assessment for Emerging Heavy-Duty Truck Powertrain Technologies in China: A Comparative Study of Battery Electric, Fuel Cell Electric, and Hydrogen Combustion Engine Trucks». In: *Environmental Science & Technology* 59.4 (Feb. 2025). Publisher: American Chemical Society, pp. 2018–2030. ISSN: 0013-936X. DOI: 10.1021/acs.est.4c11737. URL: https://doi.org/10.1021/acs.est.4c11737 (visited on 06/13/2025) (cit. on p. 6).
- [10] Achim Kampker, Rahul Pandey, Jose Guillermo Dorantes Gomez, Saskia Wessel, Patrick-Emanuel Treichel, and Ibrahim Malatyali. «Cost Optimal Design Strategy of Electric Drivetrains for Medium Heavy-Duty Vehicles Based on Product Development and Production Costs». In: 2019 9th International Electric Drives Production Conference (EDPC). 2019, pp. 1–8. DOI: 10.1109/EDPC48408.2019.9011844 (cit. on p. 6).
- [11] Sreedhar Madichetty, Avram John Neroth, Sukumar Mishra, and B. Chitti Babu. «Route Towards Road Freight Electrification in India: Examining Battery Electric Truck Powertrain and Energy Consumption». In: *Chinese Journal of Electrical Engineering* 8.3 (2022), pp. 57–75. DOI: 10.23919/CJEE. 2022.000026 (cit. on p. 7).
- [12] Marcus Auch, Timo Kuthada, Sascha Giese, and Andreas Wagner. «Influence of Lithium-Ion-Battery Equivalent Circuit Model Parameter Dependencies and Architectures on the Predicted Heat Generation in Real-Life Drive Cycles». In: *Batteries* 9.5 (May 2023). Number: 5 Publisher: Multidisciplinary Digital Publishing Institute, p. 274. ISSN: 2313-0105. DOI: 10.3390/batteries9 050274. URL: https://www.mdpi.com/2313-0105/9/5/274 (visited on 06/14/2025) (cit. on p. 8).

- [13] Magnus Lindgren. «Electric road system technologies in Sweden». In: (2020) (cit. on p. 8).
- [14] Martin G H Gustavsson, Florian Hacker, and Hinrich Helms. «Overview of ERS concepts and complementary technologies». en. In: (2019) (cit. on p. 8).
- [15] Yaowen Pei, Feng Chen, Tao Ma, and Gonghui Gu. «A comparative review study on the electrified road structures: Performances, sustainability, and prospects». In: Structures 62 (Apr. 2024), p. 106185. ISSN: 2352-0124. DOI: 10.1016/j.istruc.2024.106185. URL: https://www.sciencedirect.com/science/article/pii/S2352012424003370 (visited on 06/05/2025) (cit. on pp. 8-10, 12).
- [16] Wayback Machine. Aug. 2020. URL: https://web.archive.org/web/20200803034309/https://trl.co.uk/sites/default/files/PIARC%20ERS%20Academy%20Report%20PPR875_Final%20Version.pdf (visited on 06/05/2025) (cit. on pp. 10, 11).
- [17] Electric Road Systems, ERS. en-US. May 2021. URL: https://f3centre.se/en/fact-sheets/electric-road-systems-ers/ (visited on 06/05/2025) (cit. on p. 10).
- [18] Laura Soares and Hao Wang. «A study on renewed perspectives of electrified road for wireless power transfer of electric vehicles». In: Renewable and Sustainable Energy Reviews 158 (Apr. 2022), p. 112110. ISSN: 1364-0321. DOI: 10.1016/j.rser.2022.112110. URL: https://www.sciencedirect.com/science/article/pii/S1364032122000399 (visited on 06/05/2025) (cit. on pp. 10-12).
- [19] Mauro Feliziani, Tommaso Campi, Silvano Cruciani, and Francesca Maradei. «Introduction to wireless power transfer for e-mobility». en. In: Wireless Power Transfer for E-Mobility. Elsevier, 2024, pp. 1–24. ISBN: 978-0-323-99523-8. DOI: 10.1016/B978-0-323-99523-8.00004-7. URL: https://linkinghub.elsevier.com/retrieve/pii/B9780323995238000047 (visited on 06/06/2025) (cit. on pp. 11, 12).
- [20] PRé Sustainability. SimaPro 8 Introduction to LCA. https://pre-sustainability.com/files/2014/05/SimaPro8IntroductionToLCA.pdf. Guide document by PRé Sustainability. 2014. (Visited on 06/16/2025) (cit. on p. 13).
- [21] International Organization for Standardization. ISO 14040:2021 Environmental management Life cycle assessment Principles and framework. Revised version of ISO 14040:2006. ISO. Geneva, Switzerland: International Organization for Standardization, 2021. URL: https://www.iso.org/standard/76122.html (visited on 10/11/2025) (cit. on p. 13).

- [22] International Organization for Standardization. ISO 14044:2021 Environmental management Life cycle assessment Requirements and guidelines. ISO. Geneva, Switzerland: International Organization for Standardization, 2021. URL: https://www.iso.org/standard/76123.html (visited on 10/11/2025) (cit. on p. 13).
- [23] International Organization for Standardization. ISO 14025:2010 Environmental labels and declarations Type III environmental declarations Principles and procedures. ISO. Geneva, Switzerland: International Organization for Standardization, 2010. URL: https://www.iso.org/standard/38131.html (visited on 10/11/2025) (cit. on p. 13).
- [24] Ecochain. A Quick Guide to LCA. https://mail.ecochain.com/hubfs/ Whitepapers/Ecochain_QuickGuidetoLCA.pdf. Whitepaper on Life Cycle Assessment. 2020. (Visited on 06/16/2025) (cit. on p. 13).
- [25] Lisa Ellram. «Total Cost of Ownership: An Analysis Approach for Purchasing». In: International Journal of Physical Distribution & Logistics Management 25 (Oct. 1995), pp. 4–23. DOI: 10.1108/09600039510099928 (cit. on p. 14).
- [26] Investopedia. Residual Value. Definition and explanation of residual value in finance and leasing contexts. 2025. URL: https://www.investopedia.com/terms/r/residual-value.asp (visited on 10/11/2025) (cit. on p. 14).
- [27] Corporate Finance Institute. Net Present Value (NPV). URL: https://corporatefinanceinstitute.com/resources/valuation/net-present-value-npv/ (visited on 09/16/2025) (cit. on p. 15).
- [28] Trentalessandro Costantino, Federico Miretti, and Ezio Spessa. «Assessing the viability of dynamic wireless power transfer in long-haul freight transport: A techno-economic analysis from fleet operators' standpoint». In: Applied Energy 379 (2025), p. 124839. ISSN: 0306-2619. DOI: https://doi.org/10.1016/j.apenergy.2024.124839. URL: https://www.sciencedirect.com/science/article/pii/S0306261924022220 (cit. on pp. 15, 17, 20, 21, 35, 58, 59).
- [29] Comité National Routier (CNR). Italian Road Freight Transport Sector 2021. Paris, France: Comité National Routier, 2021. URL: https://www.cnr.fr/en/italian-road-freight-transport-sector-2021 (visited on 10/11/2025) (cit. on p. 15).
- [30] Persyn D, Diaz Lanchas J, and Barbero Jimenez J. Estimating road transport costs between EU regions. Scientific analysis or review. Brussels (Belgium), 2019. URL: https://publications.jrc.ec.europa.eu/repository/handle/JRC114409 (cit. on p. 15).

- [31] Felipe Rodríguez, Nic Lutsey, and Oscar Delgado. Total Cost of Ownership for Tractor-Trailers in Europe: Battery Electric Versus Diesel. Washington, D.C.: The International Council on Clean Transportation (ICCT), 2023. URL: https://theicct.org/publication/total-cost-of-ownership-for-tractor-trailers-in-europe-battery-electric-versus-diesel/(visited on 10/11/2025) (cit. on p. 15).
- [32] Eamonn Mulholland and Hussein Basma and Pierre-Louis Ragon and Felipe Rodríguez. Within Reach: The 2025 CO₂ Targets for New Heavy-Duty Vehicles in Europe. International Council on Clean Transportation, 2025. URL: https://theicct.org/wp-content/uploads/2025/09/ID-456-%E2%80%93-EU-HDV-Targets_report_final.pdf (visited on 10/11/2025) (cit. on p. 19).
- [33] European Automobile Manufacturers' Association (ACEA). Preliminary CO_2 baseline for heavy-duty vehicles. Brussels, Belgium: ACEA, 2020. URL: https://www.acea.auto/files/ACEA_preliminary_CO2_baseline_heavy-duty_vehicles.pdf (visited on 10/11/2025) (cit. on p. 19).
- [34] IVECO S.p.A. IVECO to produce and market its Heavy-Duty Battery Electric Vehicle and Heavy-Duty Fuel Cell Electric Vehicle under its own brand. Accessed: 2025-10-11. IVECO S.p.A., 2023. URL: https://www.iveco.com/global/Press/PressReleases/2023/IVECO-to-produce-and-market-its-Heavy-Duty-Battery-Electric-Vehicle-and-Heavy-Duty-Fuel-Cell-Electric-Vehicle (cit. on p. 19).
- [35] Scania Group. Battery Electric Truck. Accessed: 2025-10-11. Scania Group, 2025. URL: https://www.scania.com/uk/en/home/products/trucks/battery-electric-truck.html (cit. on p. 19).
- [36] GraphHopper. *GraphHopper Maps*. https://graphhopper.com/maps. Accessed: 2025-06-11. 2025 (cit. on p. 22).
- [37] The MathWorks, Inc. MATLAB, version R2024a. https://www.mathworks.com/products/matlab.html. Accessed via academic license. Natick, Massachusetts, United States, 2024. (Visited on 06/16/2025) (cit. on p. 22).
- [38] Art. 142. * Limiti di velocità. it. Sept. 2023. URL: http://www.aci.it/i-servizi/normative/codice-della-strada/titolo-v-norme-di-comportamento/art-142-limiti-di-velocita.html (visited on 06/11/2025) (cit. on p. 23).
- [39] Unione Europea. Regolamento (UE) 2020/1054 del Parlamento europeo e del Consiglio del 15 luglio 2020 che modifica i regolamenti (CE) n. 561/2006 e (UE) 165/2014. Gazzetta ufficiale dell'Unione europea, L 249/1, 31 luglio 2020. Accessed 11 June 2025. 2020. URL: https://eur-lex.europa.eu/legal-content/IT/TXT/?uri=CELEX%3A32020R1054 (cit. on p. 24).

- [40] Council of the European Union. Position (EU) No PE-25-2023 Proposal for a Regulation of the European Parliament and of the Council on CO_2 emission standards for heavy-duty vehicles. Brussels, Belgium, 2023. URL: https://data.consilium.europa.eu/doc/document/PE-25-2023-INIT/en/pdf (visited on 10/11/2025) (cit. on p. 24).
- [41] Vahid Akbari, Bülent Çatay, and İhsan Sadati. «Route optimization of battery electric vehicles using dynamic charging on electrified roads». en. In: Sustainable Cities and Society 109 (Aug. 2024). Publisher: Elsevier BV, p. 105532. ISSN: 2210-6707. DOI: 10.1016/j.scs.2024.105532. URL: https://linkinghub.elsevier.com/retrieve/pii/S2210670724003585 (visited on 07/16/2025) (cit. on p. 29).
- [42] PRé Sustainability. SimaPro, version 9.5. https://simapro.com. LCA software tool by PRé Sustainability. Amersfoort, The Netherlands, 2024. (Visited on 06/16/2025) (cit. on p. 35).
- [43] Ente Nazionale Italiano di Unificazione (UNI). UNI EN 13108-1:2016 Miscele bituminose Specifiche dei conglomerati bituminosi Parte 1: Concreto bituminoso. Norma tecnica italiana. Recepimento della norma europea EN 13108-1:2006+A1:2013. 2016 (cit. on p. 37).
- [44] European Committee for Standardization (CEN). EN 1097-6:2013 Tests for mechanical and physical properties of aggregates Part 6: Determination of particle density and water absorption. European Standard. Standard applicable to aggregates used in road and civil engineering works. 2013 (cit. on p. 38).
- [45] European Committee for Standardization (CEN). EN 12591:2009 Bitumen and bituminous binders Specifications for paving grade bitumen. European Standard. Defines requirements for paving grade bitumen used in road construction. 2009 (cit. on p. 38).
- [46] European Committee for Standardization (CEN). EN 12620:2002+A1:2008 Aggregates for concrete. European Standard. Specifies properties and requirements for aggregates in concrete production. 2008 (cit. on p. 38).
- [47] Electric Vehicle Transportation Center Project (EVTCP). Task 26: Wireless Power Transfer for Electric Vehicles Final Report. https://evtcp.org/wp-content/uploads/2024/09/Task26_Final_Report.pdf. IEA HEV TCP Task 26 Wireless Power Transfer. 2024. (Visited on 06/16/2025) (cit. on p. 40).

- [48] Benedetta Marmiroli, Giovanni Dotelli, and Ezio Spessa. «Life Cycle Assessment of an On-Road Dynamic Charging Infrastructure». en. In: *Applied Sciences* 9.15 (Jan. 2019). Number: 15 Publisher: Multidisciplinary Digital Publishing Institute, p. 3117. ISSN: 2076-3417. DOI: 10.3390/app9153117. URL: https://www.mdpi.com/2076-3417/9/15/3117 (visited on 06/02/2025) (cit. on pp. 41-44, 46).
- [49] Perry Jones, Omer C. Onar, Michael Simpson, Michael Starke, and Cliff White.
 «Impact of Wireless Power Transfer Technology on Electric Vehicle Efficiency and Emissions». In: Oak Ridge National Laboratory White Paper (2014).
 Originally prepared for the IEEE International Electric Vehicle Conference (IEVC), 2014. URL: https://teem.ornl.gov/documents/publications/2014_IEVC_Impact%20of%20WPT%20v%2011%2007%202014%20v7_Jones_Onar%20v4_cleaned_up.pdf (visited on 06/16/2025) (cit. on p. 44).
- [50] Karl B. Olsson. Slide-in Electric Road System: From Idea to Project. https://www.diva-portal.org/smash/get/diva2:1131846/FULLTEXT02.pdf. Technical report available via DiVA portal. 2013. (Visited on 06/16/2025) (cit. on p. 44).
- [51] Zicheng (Kevin) Bi. «Static and Dynamic Modeling of an Inductively Coupled Power Transfer System for Electric Vehicle Applications». Master's thesis. University of Michigan, 2015. URL: https://deepblue.lib.umich.edu/bitstream/handle/2027.42/110984/Bi,%20Zicheng%20(Kevin)%20-%20Thesis%20April%202015.pdf?sequence=1 (visited on 06/16/2025) (cit. on pp. 44, 45).
- [52] Zicheng Bi, Gregory A. Keoleian, Zhenhong Lin, Michael R. Moore, Kainan Chen, Lingjun Song, and Zhengming Zhao. «Life cycle assessment and tempospatial optimization of deploying dynamic wireless charging technology for electric cars». en. In: Transportation Research Part C: Emerging Technologies 100 (Mar. 2019), pp. 53–67. ISSN: 0968090X. DOI: 10.1016/j.trc.2019.01. 002. URL: https://linkinghub.elsevier.com/retrieve/pii/S0968090X 1830740X (visited on 07/02/2025) (cit. on p. 44).
- [53] N. Di Vittorio, A. Accardo, E. Spessa, L. Viscido, et al. «LCA and LCC of a Liion Battery Pack for Automotive Application». In: *SAE International Journal of Advances and Current Practices in Mobility* 6.4 (2024), pp. 1995–2004. DOI: 10.4271/2023-24-0170. URL: https://doi.org/10.4271/2023-24-0170 (cit. on p. 55).
- [54] Luke Hutchinson, Ben Waterson, Bani Anvari, and Denis Naberezhnykh. «Potential of wireless power transfer for dynamic charging of electric vehicles». In: *IET Intelligent Transport Systems* 13.1 (2019), pp. 3–12. ISSN: 1751-9578. DOI: 10.1049/iet-its.2018.5221. URL: https://onlinelibrary.wiley.

- com/doi/abs/10.1049/iet-its.2018.5221 (visited on 09/21/2025) (cit. on p. 58).
- [55] Jasprit S. Gill, Parth Bhavsar, Mashrur Chowdhury, Jennifer Johnson, Joachim Taiber, and Ryan Fries. «Infrastructure Cost Issues Related to Inductively Coupled Power Transfer for Electric Vehicles». In: *Procedia Computer Science* 32 (2014), pp. 545–552. ISSN: 18770509. DOI: 10.1016/j.procs. 2014.05.459. URL: https://linkinghub.elsevier.com/retrieve/pii/S1877050914006590 (visited on 08/23/2025) (cit. on p. 58).